CNRS
Centre National de la Recherche Scientifique

INFN
Istituto Nazionale di Fisica Nucleare

AdV INJ: Mode matching telescope configuration choice for the ITF input telescope.

VIR-0010B-12

M. Barsuglia, C. Buy, B. Canuel, R. Day, E. Genin, J. Marque, G. Vajente

Issue: 1

Date: February 3, 2012

VIRGO * A joint CNRS-INFN Project
Via E. Amaldi, I-56021 S. Stefano a Macerata - Cascina (Pisa)
Secretariat: Telephone (39) 050 752 521 * FAX (39) 050 752 550

Contents

1 Introduction

The aim of this document is to explain why we have chosen the catadioptric telescope as mode matching telescope (MMT) for the input MMT of AdV respect to the reflective one. First, general requirements on the ITF MMT are given. Then, both configurations are presented as well as the trade-off studies to make a decision on the configuration we chose to adopt for AdV. Mainly, a tolerancing study and the computation of diffused light noise for both configurations and back-reflected noise for the most specific case of the meniscus lens used in the catadioptric telescope are presented here.

2 General requirements

The general requirements of the ITF MMT are given in table 1.

Parameter	Requirement
Mode matching (on the ITF)	$\geq 99\%$
Noise coming from diffused and back-reflected light	$\leq$ AdV sensitivity/10
Magnification	38 (expected to be decreased down to 19)
Telescope dimensions	$<$ 800mmX350mm

Table 1: ITF MMT requirements.

General considerations.
Considering manufacturing errors on optical elements parameters (radius of curvature, surface deviation,...) and alignment errors, the telescope should have the capacity to recover a good matching ($> 99\%$ as said above).
Finally, the magnification of the telescope should be sufficient to separate properly the secondary beams coming from the ITF with respect to the main beam (depends on pick-off beams angle of incidence at the MMT input) (see OSD chapter for this particular point).

3 Catadioptric and reflective telescopes: Overview, performances and tolerancing study

3.1 Overview of 2 possible configurations

Configuration 1: *Catadioptric mode matching telescope*

This telescope has been proposed at the beginning of the design work on MSRC configuration for AdV that has started in February 2011[1][2]. The design choice has been driven by the space constraints on the Suspended Injection Bench and the fact that we had to reduce as much as possible aberrations of the telescope since the Power Recycling(PR) mirror Anti-Reflective (AR) face has to be curved as we cannot install large optics on this bench. We considered an afocal telescope (similar to Virgo ITF MMT) that increases the beam size by a factor of 16 (from 1.3 to 21mm). Then a diverging lens is used in combination of PR mirror to match the beam on the interferometer. The big interest of this configuration is that it is implementable on a bench that is not bigger than the one currently used in Virgo. The compactness of the telescope is an advantage for the design of Suspended Injection Bench (SIB) considering that we will have a lot of cumbersome elements to install on it (Faraday isolator, Reference cavity, dihedron, Input Power control system). The shape of the diverging lens has been chosen and optimized in order to compensate spherical aberrations induced by the recycling mirror. This optimization enables us to reach by design a very good matching of the input beam on the interferometer (higher than 99.9%).

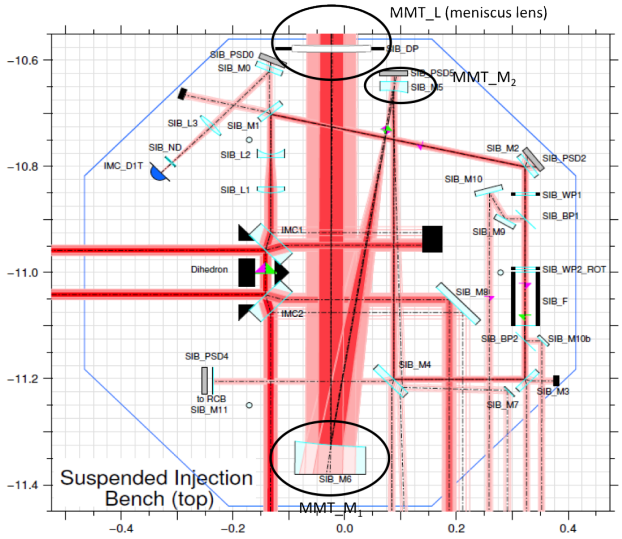

Figure 1: Virgo Suspended Injection Bench layout where one can see a possible position for the meniscus lens MMT_L.

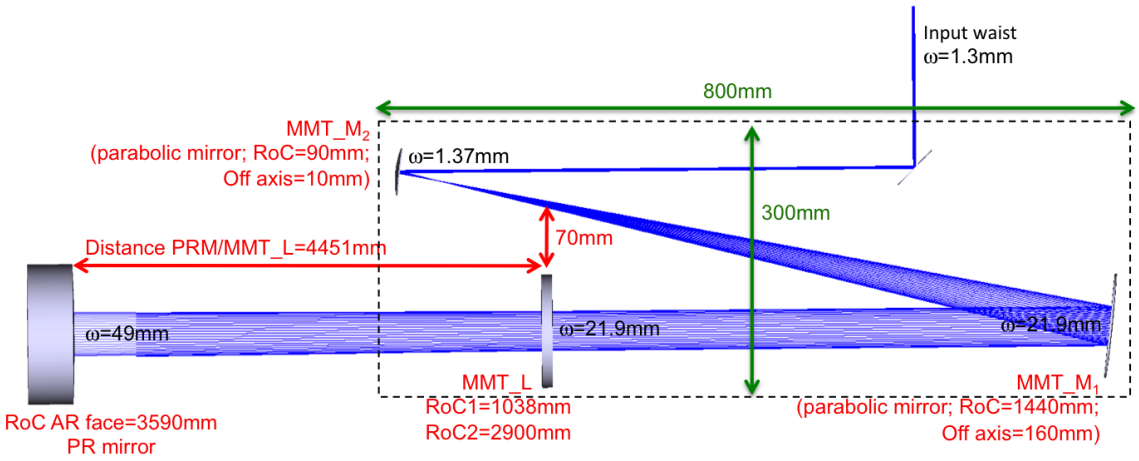

Figure 2: Overview of the catadioptric telescope.

The telescope magnification has been optimized in order to easily separate the pick-off beams as explained in [3]. The input beam waist size is about 1.3 mm in the configuration that is presented in this document (see figure 2). In this configuration the dimension of the telescope can be estimated to be around 80 cmx30 cm taking into account the opto-mechanical mounts (to be compared with Virgo SIB parabolic off-axis telescope that can be placed in a rectangle of 70 cmx25 cm).

NB: final optimization of the telescope is needed since very recently OSD subsystem has confirmed the wedge angle for beam splitter mirror. It is likely that we will be able to relax the magnification of telescope keeping

enough separation between the main beam and the pick-offs. Our goal is to reduce the magnification of the telescope by a factor of 2.

Configuration 2:

An alternative design has been also studied [4] that uses only reflecting optics on the benches at the cost of having a bit less compact telescope. The main interest of this configuration is to avoid the direct back-reflection due to AR coating of refractive optics. A view of this reflective telescope is presented on the figure 3. The first

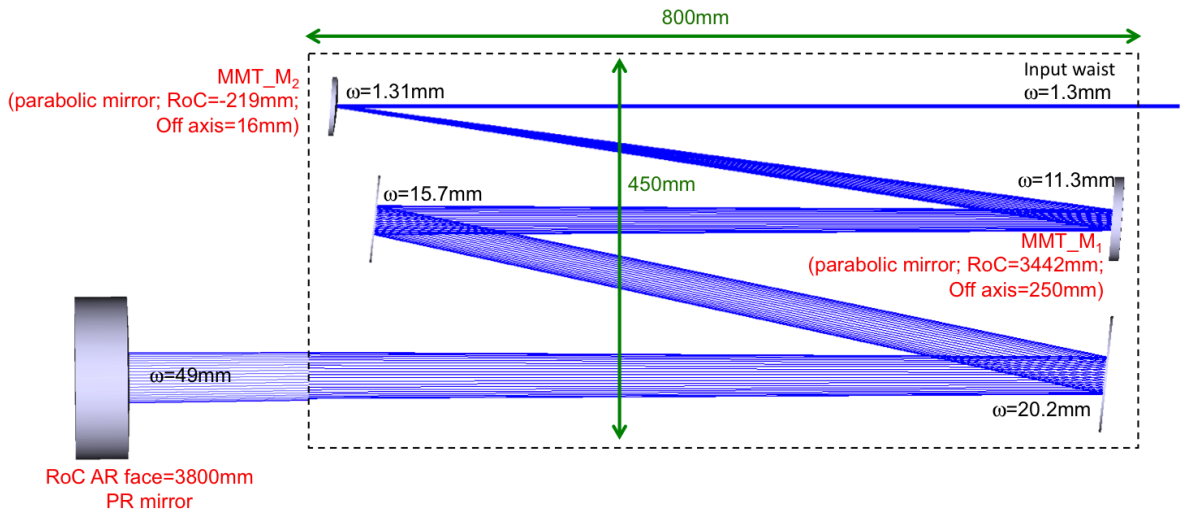

Figure 3: Overview of the reflective telescope.

element of the telescope is the curved face of PR mirror, used to reduce the size of the beam on the bench. Two flat mirrors are first placed on the bench to increase the optical path length between the recycling mirror and the first parabolic mirror (MMT_M_1) in order to reduce as much as possible spherical aberrations of the optical system. Then, two off-axis parabolic mirrors are used in non-afocal configuration to adjust the beam size to 1.3 mm waist on the SIB faraday isolator. It is important to note that other mirror shapes (spherical, hyperbolic and elliptic) have been studied without good results. The minimum space needed for this telescope is 80 cmx45 cm taking into account the opto-mechanical mounts.

3.2 Mode matching performance

As shown in figure 4, a matching of the beam on the interferometer higher than 99.9% is achieved with the catadioptric telescope. This is mainly due to the fact that this configuration has very low aberrations since the parabolic off-axis telescope is used in afocal configuration and that the role of the meniscus lens is to compensate for spherical aberrations introduced by the curved face of PR mirror.

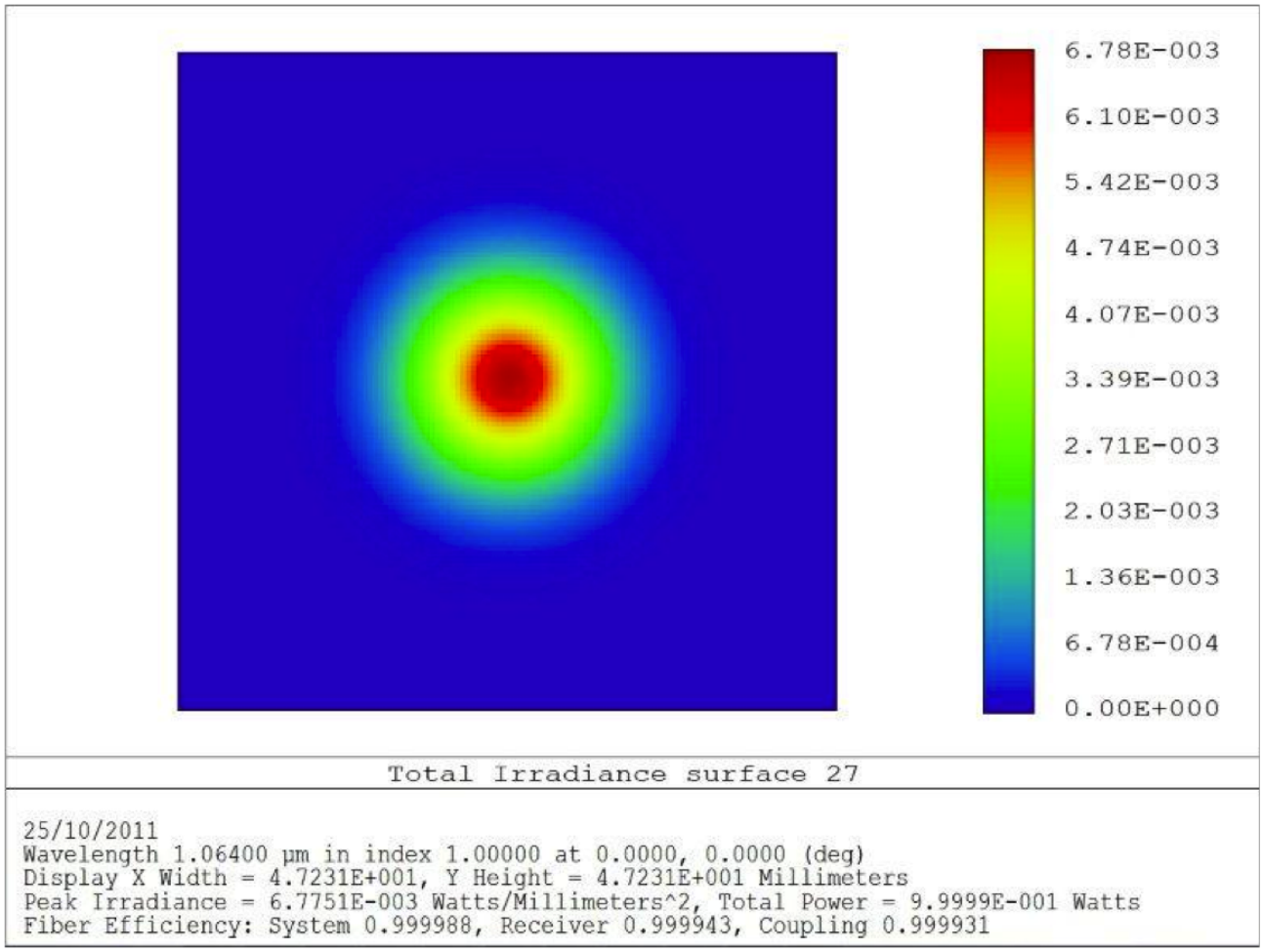

Figure 4: Coupling of the beam in the interferometer using the catadioptric telescope (FFT propagation with Zemax). A matching higher than 99.9% is achieved.

For the reflective telescope, the two parabolic mirrors are not placed in an afocal configuration. The two flat mirrors are used to increase the optical path length and reduce the spherical aberrations induced by the AR face of PR mirror. However, remaining aberrations in the optical system, mainly spherical aberrations and astigmatism, are present. The shape of the beam is plotted on the figure 5 as well as the coupling efficiency that is of the order of 99.5%.

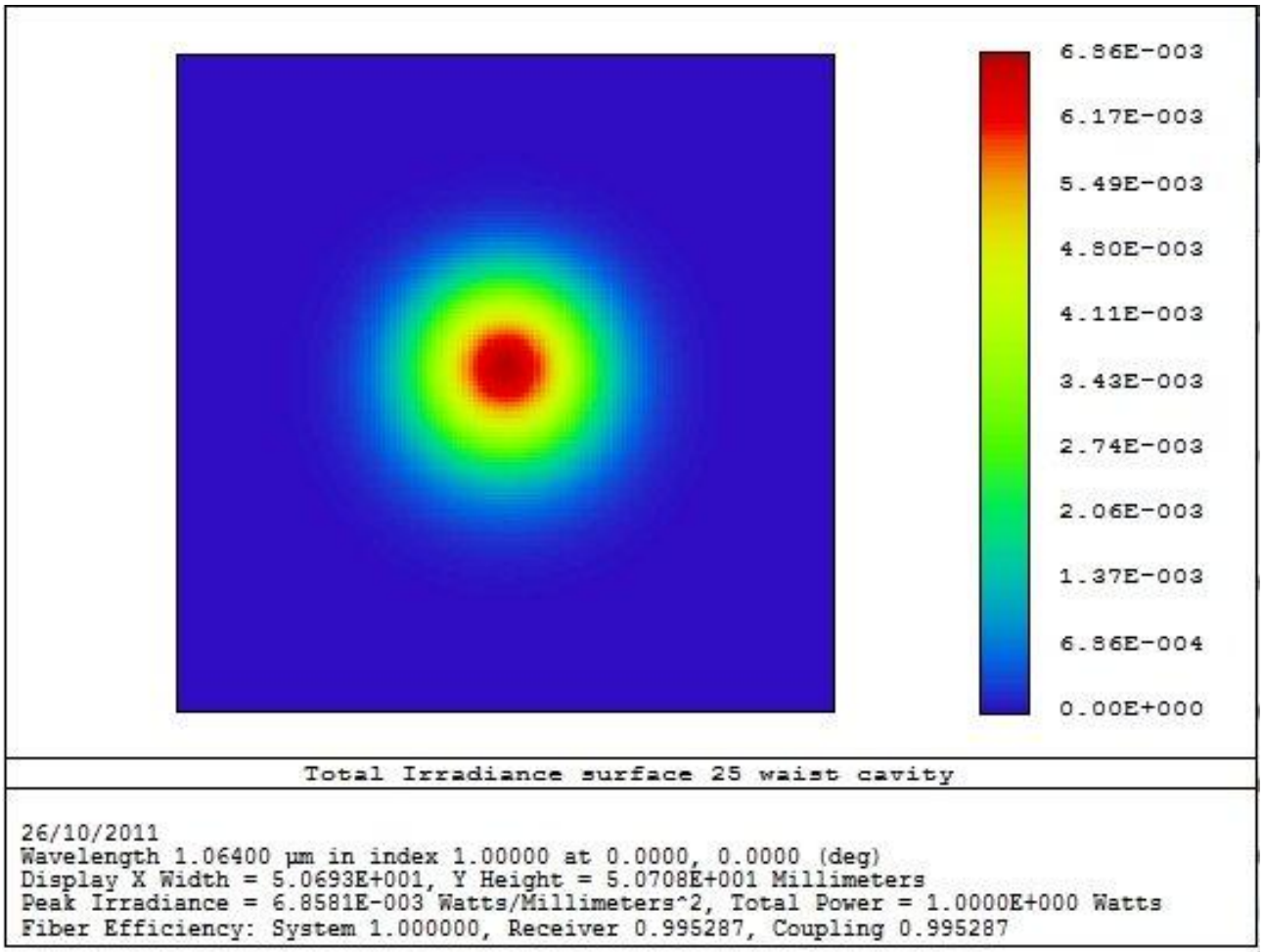

Figure 5: Coupling of the beam in the interferometer using the reflective telescope (FFT propagation with Zemax). A matching higher than 99.5% is achieved.

3.3 Tolerancing study of radius of curvatures

Definition of the tolerancing study

The tolerancing study was performed using the Zemax software (Monte Carlo simulation method). The aim is to find the most critical parameters of the optical system that contribute to the system performances worsening, and define the good compensators to recover optimal performances. This analysis is powerful and useful because all the tolerances can be considered at once. Every parameter is randomly perturbed using appropriate statistical models, all compensators are adjusted and the entire system is evaluated with all defects considered.

First, we define a merit function that describes the coupling efficiency. This function is built considering errors on beam waist with respect to the ideal size, error on beam position with respect to ideal position and the remaining aberrations such as spherical aberrations, coma and astigmatism. The merit function value is close to 0 at the optimal configuration implying a coupling efficiency of 99.9% for the catadioptric telescope and 99.5% for the reflective telescope.

We considered errors on the surface of the optics of the telescopes: the radii of curvature (RoCs) and the surface irregularities. The errors given by the manufacturers on the RoCs of the mirrors are of the order of +/-1%,

Optical element	RoC value (mm)
MMT_M_1	1440 +/- 14.4
MMT_M_2	90 +/- 0.9
MMT_L_1	2900 +/- 29
MMT_L_2	1038 +/- 11
PR_AR	3590 +/- 36

Table 2: RoC errors for the tolerancing study of the catadioptric telescope.

Optics	RoC value (mm)
MMT_M_1	3442 +/- 35
MMT_M_2	- 219 +/- 22
PR_AR	3800 +/- 38

Table 3: RoC errors for the tolerancing study of the reflective telescope.

and the accuracy on the Peak-to-Valley (PtV) surface irregularities of the order of $\lambda/5$. We define such an error on the parabolic mirror surfaces, which means for the surface defects, that the irregularities are half spherical aberrations and half astigmatism. We define such errors for the optics of the telescopes. Table 2 shows the errors on the RoCs considered for the catadioptric telescope optics. Without defining any compensators, the worst offender is the RoC of the second face of the meniscus lens. The worst value of the merit function is 422, which means that the coupling efficiency falls below 40%. Then, we define compensators in order to compensate these errors and recover an optimal matching in the interferometer. For the catadioptric telescope, we can play with the distance between the two parabolic mirrors and the distance between the meniscus lens and the PR mirror. Using these compensators, the worst parameter is still the RoC of the second face of the meniscus lens but we are able to recover a merit function value of 1.9, which means a coupling efficiency higher than 99.8%.

Table 3 shows the errors on the RoCs of the optics of this reflective telescope. Without using compensator the most influent parameter is the RoC of the AR PR mirror and the merit function value is 478 which means, as for the catadioptric telescope, that the coupling efficiency is lower than 40%. To compensate these errors, we can use only one compensator in this case, which is the distance between the two parabolic mirrors. Using that distance, the most degrading parameter are the surface irregularities of MMT_M_1 and we can recover a merit function value of 32 which imply a coupling efficiency not better than 92%. As we will see in details hereafter, the RoCs errors of the optics of the reflective telescope can be compensated by using the distance between the two parabolic mirrors, but the surface irregularities, and in particular the defects of MMT_M_1, cannot be compensated enough to recover a coupling efficiency higher than 99%.

Radius of Curvature (RoC) of the optics

We have seen that the RoC errors can be compensated for the two configurations. We studied separately the RoC errors of each optics of the telescopes in order to confirm this previous result and define the maximum ranges of the compensators.

On the figure 6 is plotted the coupling of the input beam with the ITF as a function of the MMT_M_1 RoC and on figure 7 MMT_M_2 RoC and the distance between the two parabolic mirrors, for the catadioptric telescope. We can see that if the RoC of the mirrors varies by +/- 1%, we are able to recover an optimal coupling by adjusting the distance between the 2 parabolic mirrors. On the figures 8 and 9, we can see that same results are obtained by using another compensator, the distance between the PR mirror and the meniscus lens.

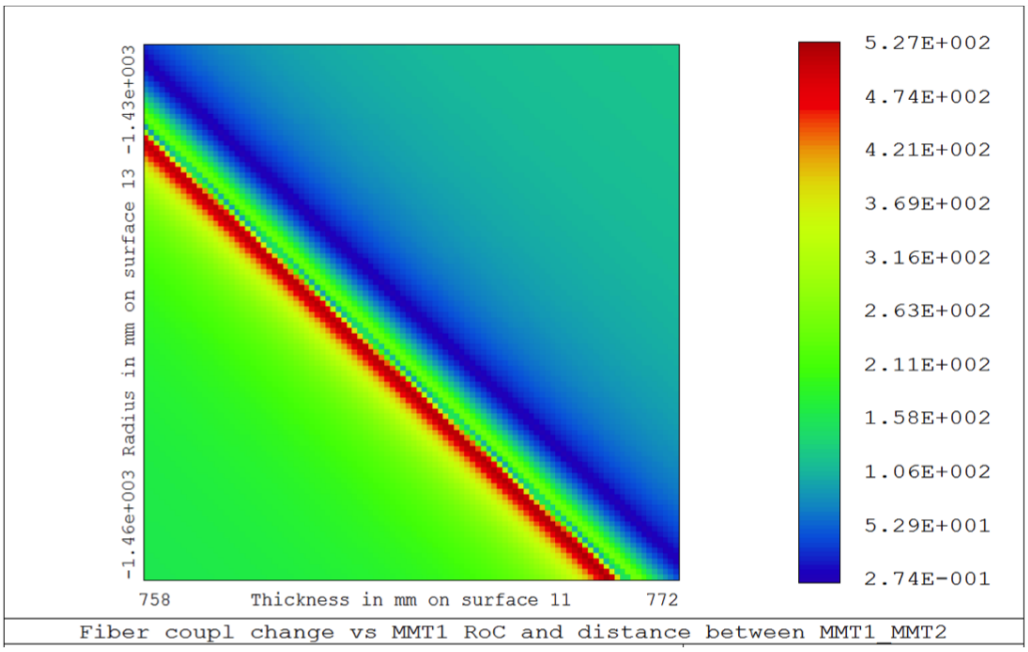

Figure 6: Coupling efficiency as a function of the MMT_M_1 RoC and the distance between the two parabolic mirrors, for the catadioptric telescope.

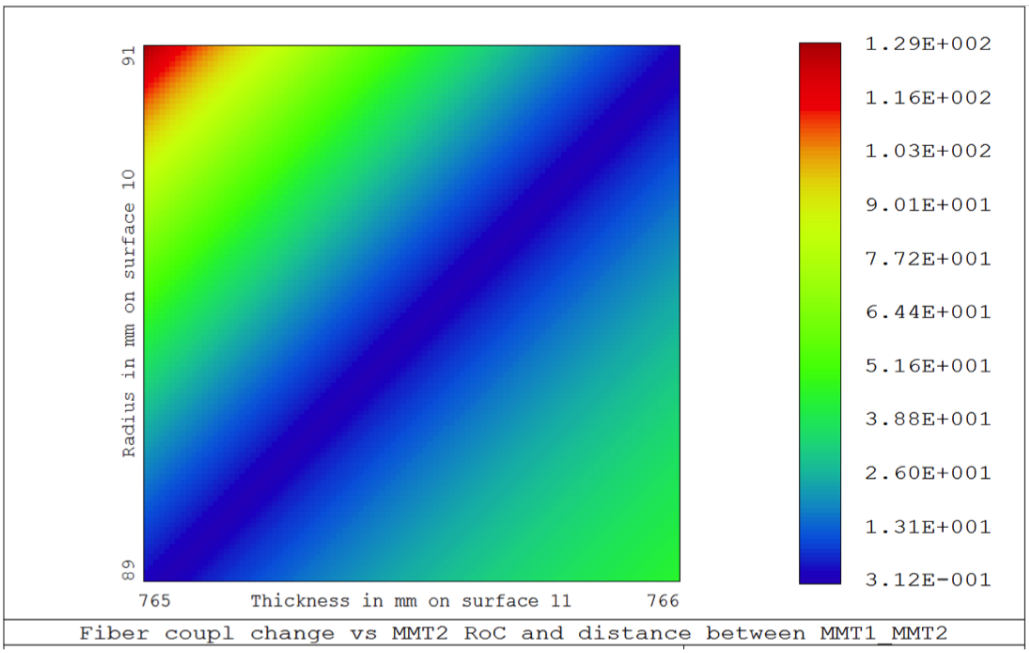

Figure 7: Coupling efficiency as a function of the MMT_M_2 RoC (right) and the distance between the two parabolic mirrors, for the catadioptric telescope.

Same kind of study has been made for the PR mirror and the meniscus lens. Similar errors have been used for the RoC of these optics, even if the PR mirror AR face will have an accuracy better than 1%. Figures 10 and 11 show the coupling of the main beam with the ITF as a function of the MMT_L_1 RoC (left) and MMT_L_2 RoC (right) and the distance between the two parabolic mirrors. On the figure 12 is plotted the coupling of

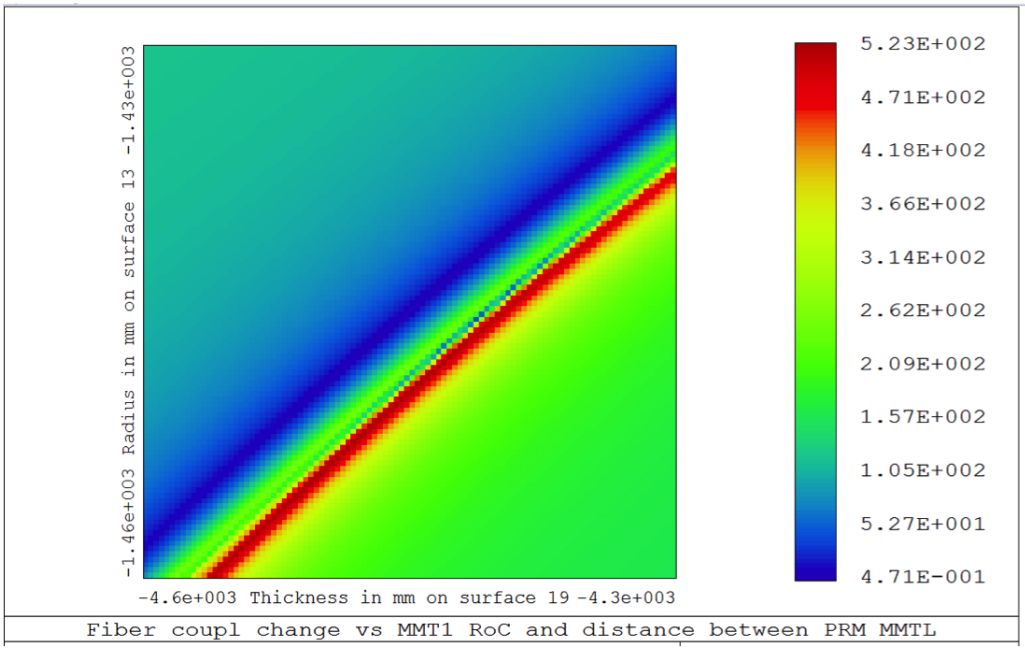

Figure 8: Coupling efficiency as a function of the MMT_M_1 RoC and the distance between PR mirror and the meniscus lens, for the catadioptric telescope.

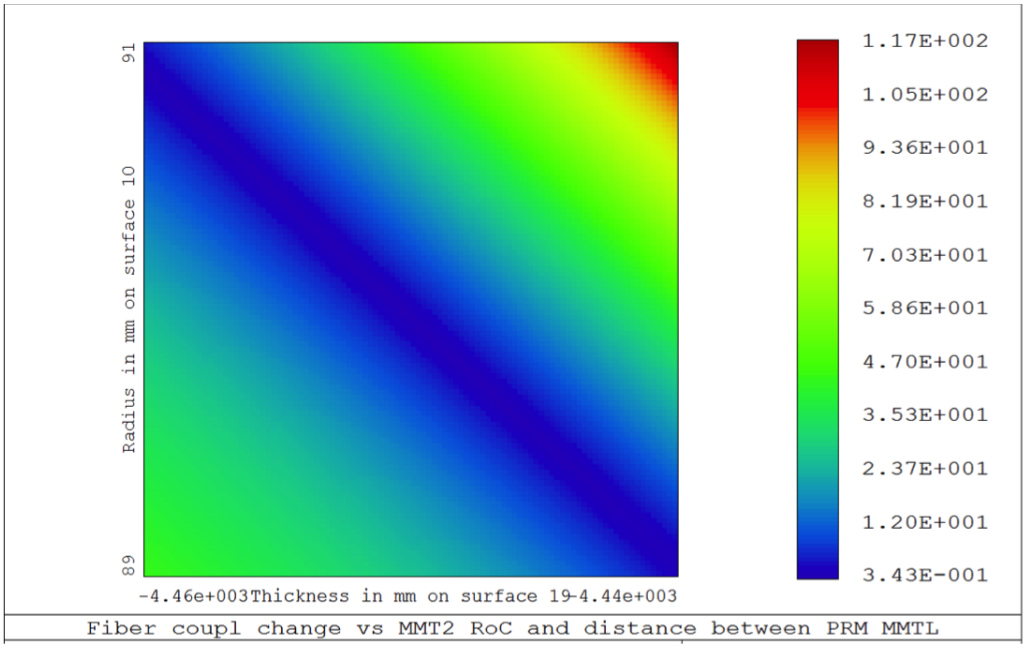

Figure 9: Coupling efficiency as a function of the MMT_M_2 RoC (right) and the distance between PR mirror and the meniscus lens, for the catadioptric telescope.

the main beam with the ITF as a function of the PRM AR RoC and the distance between the two parabolic mirrors.

Note that same results are obtained by adjusting the distance between the PR mirror and the meniscus lens. Table 4 summarizes the ranges of the compensators necessary to compensate separately each RoC errors of the

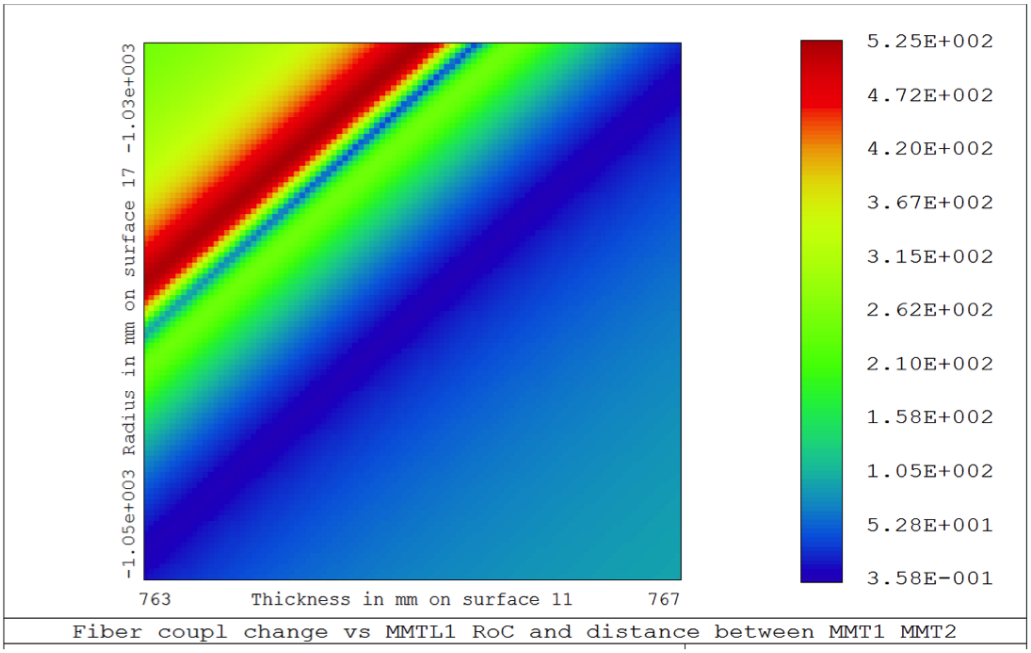

Figure 10: Coupling efficiency as a function of the MMT_L_1 RoC (left) and the distance between the two parabolic mirrors, for the catadioptric telescope.

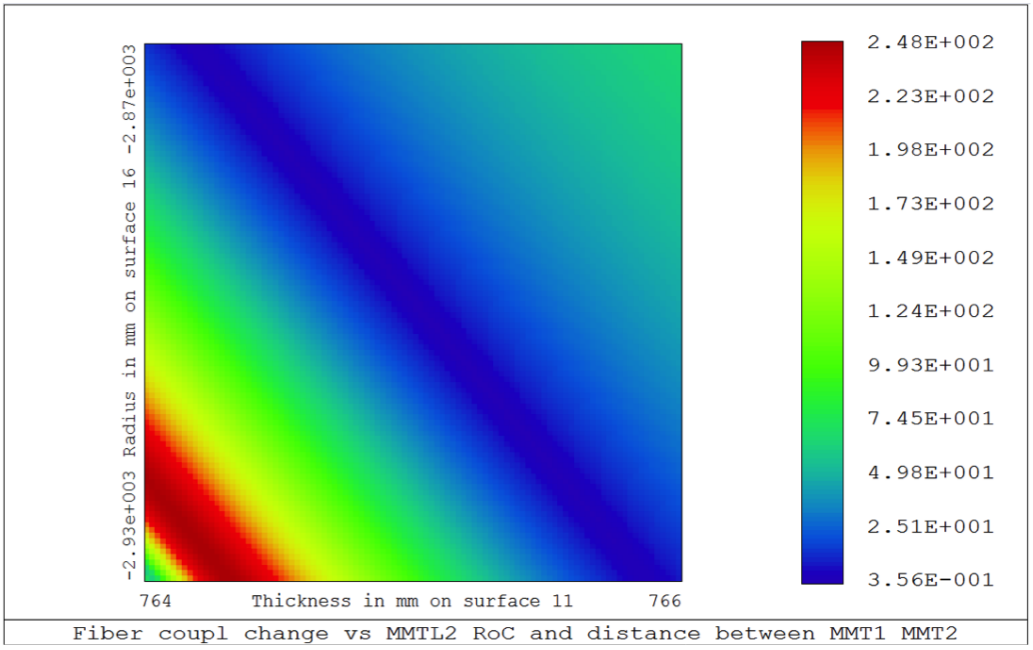

Figure 11: Coupling efficiency as a function of the MMT_L_2 RoC (right) and the distance between the two parabolic mirrors, for the catadioptric telescope.

optics.

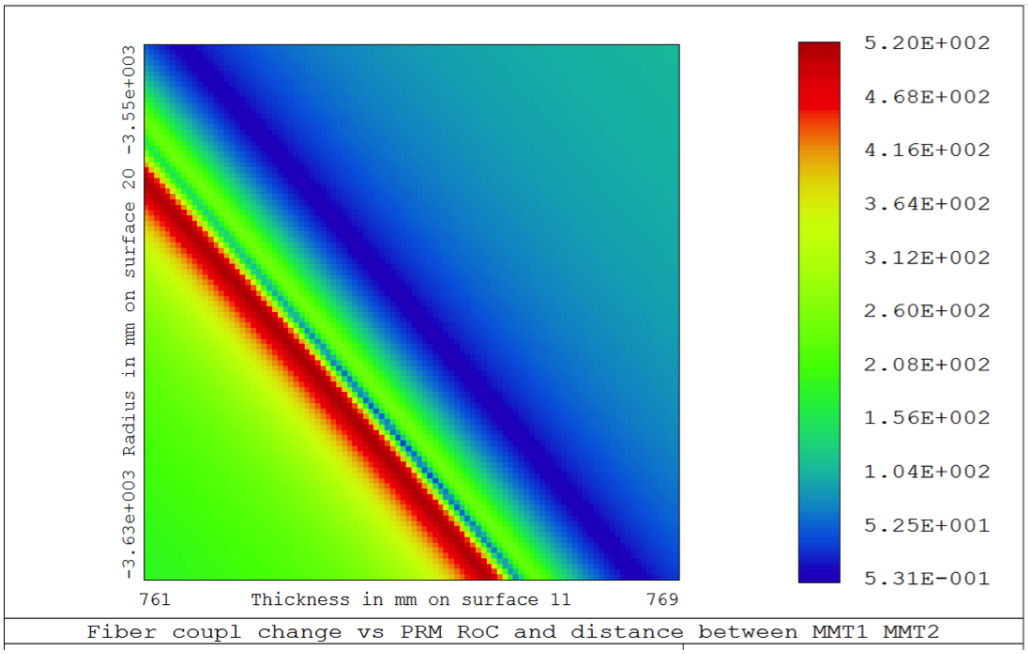

Figure 12: Coupling efficiency as a function of the PRM AR RoC and the distance between the two parabolic mirrors, for the catadioptric telescope.

Optics	MMT_M_1 / MMT_M_2 (mm)	PR_AR / MMT_L (mm)
MMT_M_1	± 7	± 150
MMT_M_2	± 0.25	± 11
MMT_L_1	± 2	± 22
MMT_L_2	± 0.5	± 50
PR_AR	± 4	± 80

Table 4: Ranges of the compensators of the catadioptric telescope necessary to compensate separately RoC errors of the optics of $\pm$ 1 %.

Note that, by playing with the two compensators, we can relax the ranges as one can see on figure 13 . The ranges defined here will help us to make the appropriate choice of actuators and in the design of the mechanical mounts of telescope'optics.

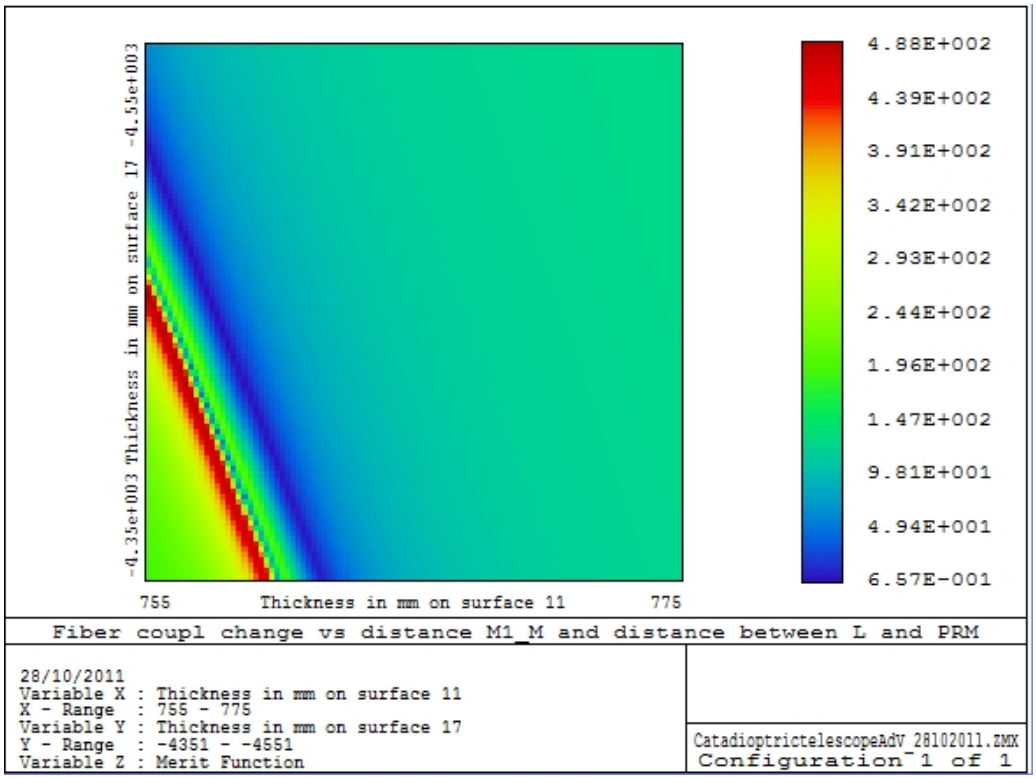

Figure 13: Coupling efficiency as a function of the distance between PR mirror and the meniscus lens (vertical axis; range=±100mm) and the distance between the two parabolic mirrors (horizontal axis ; range=±10mm), for the catadioptric telescope considering a static error of 1% on MMT_M_1 RoC.

Similar study has been performed for the reflective telescope. In this case, only one compensator is available, which is the distance between the two parabolic mirrors. The distance between the PR mirror and MMT_M_1 has to be modified by several meters before it impacts the performances of the system. The figures 14 and 15 show the coupling efficiency as a function of the MMT_M_1 RoC (left) and MMT_M_2 (right) and the distance between the two parabolic mirrors. We can see that if the RoC of the mirrors varies by +/- 1%, we are able to recover an optimal coupling by playing with the distance between the optics. The coupling efficiency as a function of the PR mirror AR RoC and the distance between the parabolic mirrors is given on figure 16. An error of +/- 1% on the PR mirror AR face could be compensated by using the distance between the optics. The table 5 summarize the ranges of the compensators necessary to compensate separately each RoC errors of the optics. In this case, only one compensator is available and we can not relax these requirements on the range of the distance MMT_M_1 / MMT_M_2.

Optics	MMT_M_1 / MMT_M_2 (mm)
MMT_M_1	±5
MMT_M_2	±2.5
PR_AR	±12.5

Table 5: Ranges of the compensators of the reflective telescope necessary to compensate separately RoC errors of the optics of ± 1 %.

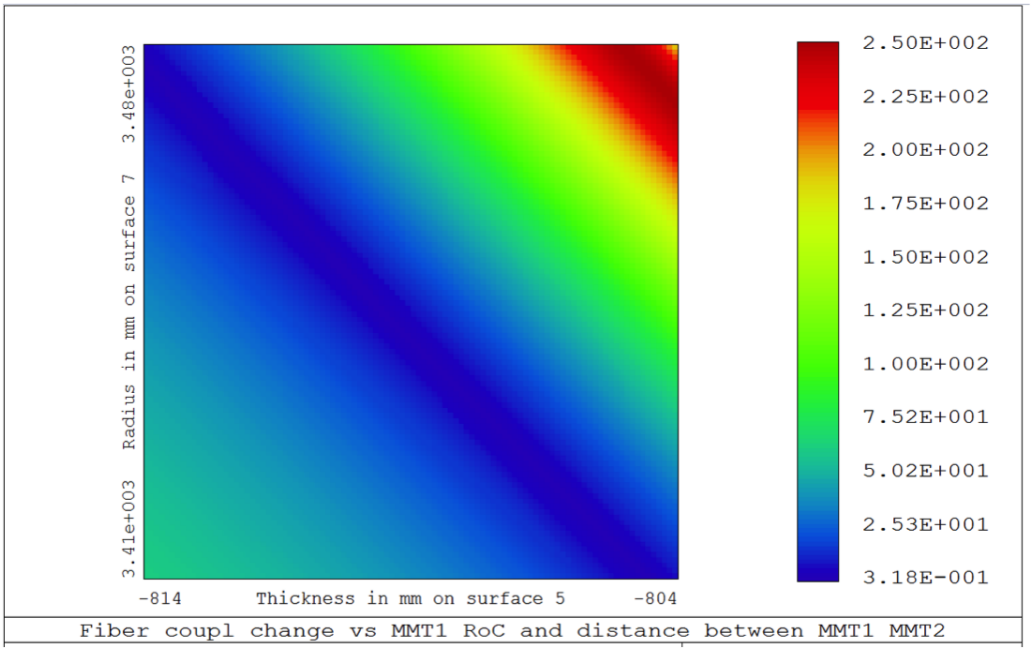

Figure 14: Coupling efficiency as a function of the MMT_M_1 RoC and the distance between the two parabolic mirrors, for the reflective telescope.

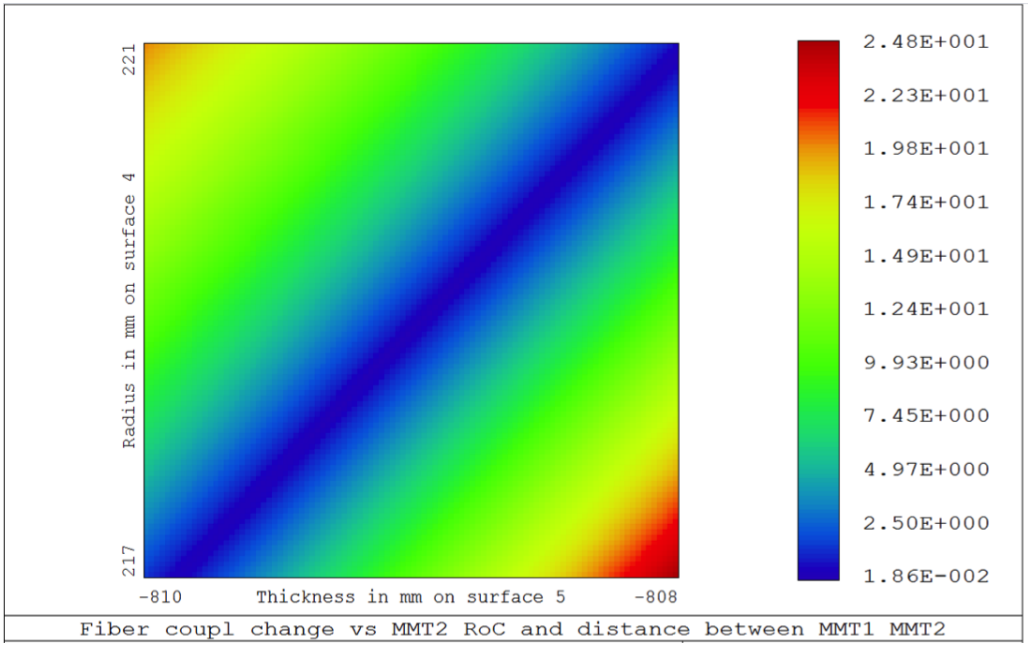

Figure 15: Coupling efficiency as a function of the MMT_M_2 RoC and the distance between the two parabolic mirrors, for the reflective telescope.

3.4 Tolerancing study for surface irregularities of the optics

As the RoC of the optics can not be perfect, their surfaces may present irregularities. Typically, the manufacturers give an accuracy on the PtV surface irregularities of the order of $\lambda/5$. We define such an error on the

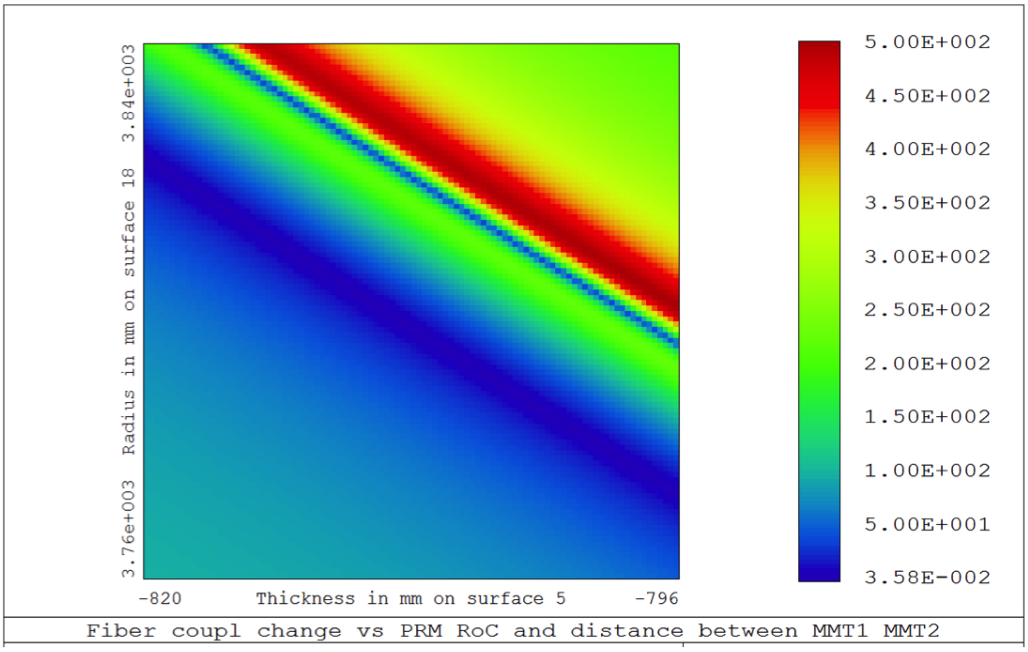

Figure 16: Coupling efficiency as a function of the PRM AR RoC and the distance between the two parabolic mirrors, for the reflective telescope.

parabolic mirror surfaces, which means, according to the Zemax software, that the irregularities are half spherical aberrations and half astigmatism. The shape of the beam is affected and the coupling with the ITF beam falls below 80% for both configurations. If we consider compensators, the distance between the two parabolic mirrors and the distance between the PR mirror and the meniscus lens, that are adjusted to correct these errors, we are able to recover a matching higher than 99.7% for the catadioptric telescope. In the case of the reflective telescope, the compensator which is the distance between the two parabolic mirrors does not allow to recover a matching higher than 92%. (part expected to be moved in another document).

3.5 Tolerancing study for input beam geometry errors

The input beam coming from the faraday isolator (FI) could present errors on the waist size, the waist position or both, and we studied the possibility to compensate such errors by adjusting a defined compensator. On the figure 17, the plots are representing the coupling of the beam in the ITF according to the distance between the PR mirror and the meniscus lens, for the catadioptric telescope. The nominal and optimal configuration is when the beam waist is 1.3 mm located in the faraday isolator. If we consider errors on the input beam waist size (4%) and input beam waist position (500 mm), we can see that it is possible to recover a matching higher than 99.9% by adjusting the distance between the PR mirror and the lens. Note that matching on the ITF can also be recovered by adjusting the distance between the two off-axis parabolic mirrors.

NB: We also gave a look to the effect of a residual thermal lens of the order of 100m induced by the Faraday isolator. The effect on the coupling in the ITF is the order of 0.1% and can be easily recovered by playing with the compensators of the catadioptric telescope as explained in the paragraph above.

Similar study was made for the reflective telescope to compensate input beam errors using the distance between the two parabolic mirrors. On the figure 18 is plotted the coupling efficiency according to the distance between MMT_M_1 and MMT_M_2. The nominal configuration allows a coupling higher than 99%. If the input beam waist size or position or both is modified, we can see that it is possible to recover a matching higher than 99% by using the compensator.

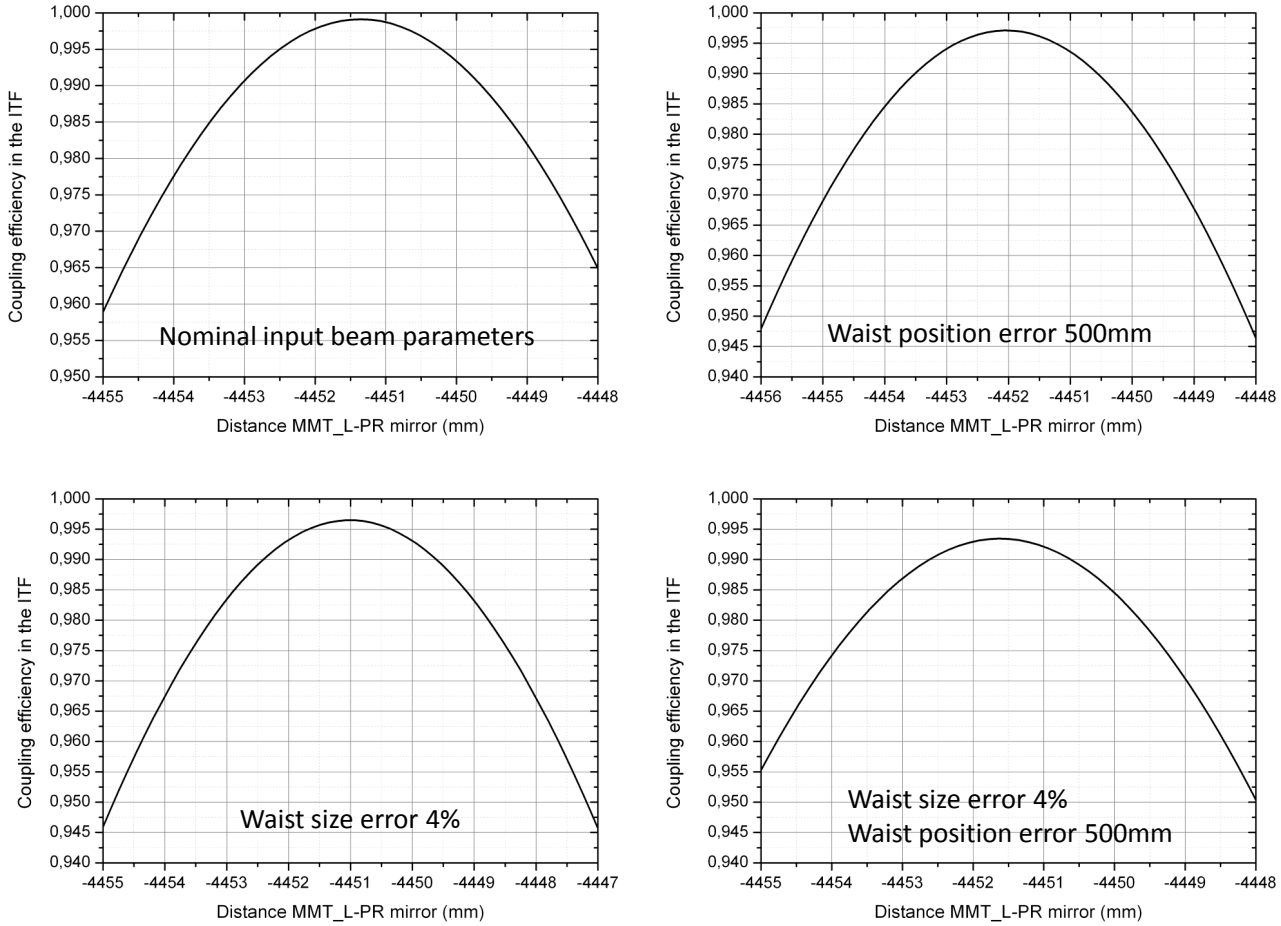

Figure 17: Coupling of the beam in the interferometer using the catadioptric telescope. A matching higher than 99% is recovered when there is an error on input beam parameters, by using the distance between the PR mirror and the meniscus lens. Nominal configuration (top left), error of 4% on the waist size (top right), error of 500 mm on the waist position (bottom left), both errors on waist size and waist position (bottom right).

3.6 Tolerancing study for tilt and decentering errors of the optics

A tilt or a decentering of the optics of the telescope will induce coma and spherical aberrations on the beam. To keep a matching of the input beam with the ITF beam higher than 99%, we computed the maximum tilt and decentering allowed on the optics mounts of the catadioptric telescope. The results are presented on the table 6. The constraints are realistic and seem manageable to what we can expect.

Moreover, we computed the shift and the tilt of the beam in the ITF as a function of the shift and the tilt of the PR mirror. The results are presented in the table 7. Assuming that the matching is higher than 99% if the beam shift in the ITF is less than 900 μm [5], it implies that the vertical and horizontal motions of the PR mirror should be smaller than 5.3 μm and the tilt motion should be smaller than 1.4 μrad, for the catadioptric telescope. These requirements for the PR mirror are not stringent, compared with alignment requirements (see alignment sectiion of ISC chapter).

Same study has been made to know the requirements for the SIB. The vertical and horizontal motions of the bench should be smaller than 5.3 μm and the tilt motion should be smaller than 1.6 μrad, for the catadioptric

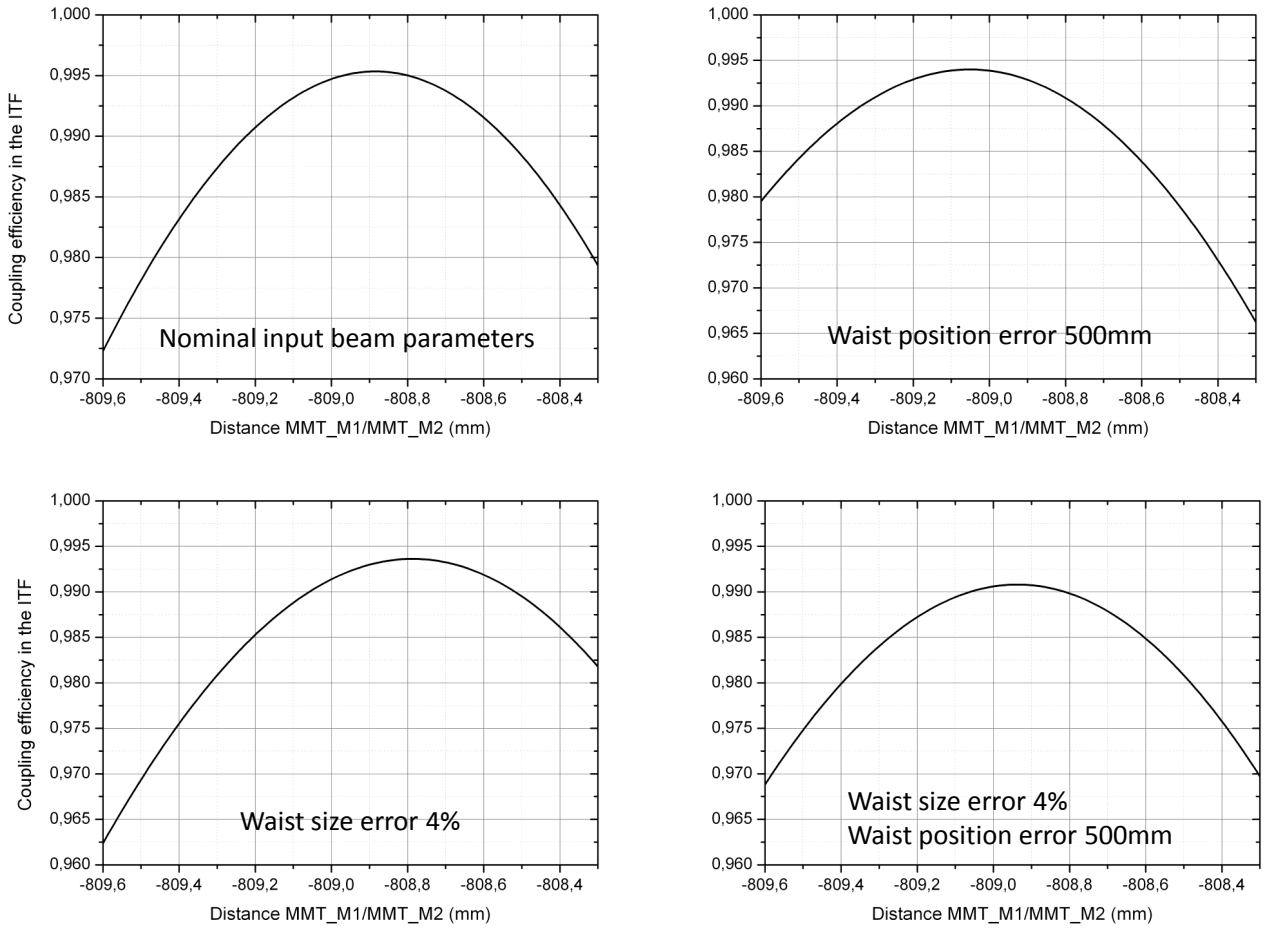

Figure 18: Coupling of the beam in the interferometer using the reflective telescope. A matching higher than 99% is recovered when there is an error on input beam parameters, by using the distance between the PR mirror and the meniscus lens. Nominal configuration (top left), error of 4% on the waist size (top right), error of 500 mm on the waist position (bottom left), both errors on waist size and waist position (bottom right).

telescope. These requirements seem to be manageable and similar to what we have currently for the Virgo SIB.

In the case of the reflective telescope, the maximum tilt and decenter allowed for the parabolic mirrors are presented in the table 8. As for the catadioptric telescope, these requirements seem realistic.

We computed also the shift and the tilt of the beam in the ITF as a function of the shift and the tilt of the PR mirror for the reflective telescope. The results are presented in the table 9. The vertical and horizontal motion of the PR mirror should be smaller than 5.6 μm and the tilt motion should be smaller than 1.1 μrad. As for the CT, these requirements for the PR mirror are not stringent, assuming that the PR mirror of current Virgo is moving much less than that. Same study has been made to know the requirements for the SIB. The vertical and horizontal motion of the bench should be smaller than 5.6 μm and the tilt motion should be smaller than 1.6 μrad, for the reflective telescope. These requirements seem to be manageable and similar to what we have currently for the Virgo SIB (see 5.2.4 and figure 38).

	MMT_M$_1$	MMT_M$_2$	MMT_L
Tilt	5 mrad	0.4 mrad	17 mrad
Decenter	300 μm	300 μm	100 μm

Table 6: Maximum tilt and decenter allowed for the optics of the catadioptric telescope, in order to keep a coupling efficiency higher than 99%.

Parameter	Value
Shift of the ITF beam vs PR motion	170μm/μm
Tilt of the ITF beam vs PR motion	1.2 $10^{-}4$ rad/μm
Shift of the ITF beam vs PR tilt	650μm/μrad
Tilt of the ITF beam vs PR tilt	1 10^{-6}rad/μrad

Table 7: Shift and tilt of the beam in the interferometer at the waist position (almost 1363 m from ITM) versus the PR mirror motion and tilt, for the catadioptric telescope. The maximum motion of the ITF beam to have a matching higher than 99% is 900 μm.

	MMT_M$_1$	MMT_M$_2$
Tilt	1.7 mrad	1.7 mrad
Decenter	300 μm	300 μm

Table 8: Maximum tilt and decenter allowed for the optics of the reflective telescope, in order to keep a coupling efficiency higher than 99%.

Parameter	Value
Shift of the ITF beam vs PR motion	160μm/μm
Tilt of the ITF beam vs PR motion	1.3 10^{-4}rad/μm
Shift of the ITF beam vs PR tilt	800μm/μrad
Tilt of the ITF beam vs PR tilt	1 10^{-6}rad/μrad

Table 9: Shift and tilt of the beam in the interferometer at the waist position (almost 1363 m from ITM) versus the PR mirror motion and tilt, for the reflective telescope. The maximum motion of the ITF beam to have a matching higher than 99% is 900 μm.

3.7 Alignment procedure

For the catadioptric telescope, there should be 2 phases in the matching adjustment. First of all, a rough adjustment/ fine alignment of the telescope will be done during the assembling phase in EGO clean rooms. This phase should be divided in 2 steps:

- Afocal parabolic telescope alignment using the procedure explained in [6].

- Alignment and rough adjustment of the meniscus lens (distance between the second parabolic mirror and the meniscus lens does not matter).

The second phase consists in performing the fine alignment when the new SIB will be installed on the interferometer. The fine tuning will be done by using 2 knobs: the distance between the 2 parabolic mirrors and the distance between PR/SR mirror and the meniscus lens. Up to now, we could not see any problem in the adjustment of the matching of the input beam with this telescope [6].

For the reflective telescope, the case is more complex. Indeed, the two parabolic mirrors are not placed in an afocal configuration. This is not a "standard" configuration for the use of such mirrors, and the alignment procedure has to be well defined and tested, which has never been made before.

4 Integration in INJ optical layout

This section should be removed from the final version of the FDR(expected to be moved in another document)

The Suspended Injection Bench (SIB) dimension for Advanced Virgo respect to Virgo is not expected to change that much. The main limitation is coming from INJ tower lower flange aperture that is of 1meter. For Advanced Virgo, the SIB diameter we have chosen for the moment is 95cm (this number could be reviewed according to the final optical layout of the SIB). As in Virgo, we plan to use the 2 planes of the breadboard itself (named upper and lower part). The optical elements that we have to install on the bench are the following:

- Ultra high vacuum Faraday isolator
- IMC flat mirrors
- Input power control system
- ITF mode matching telescope
- IMC cavity to Faraday telescope

Taking these conditions in considerations, we have tried to compare the space occupied by all these components respect to the area available on the bench for both telescope configurations. The result of this comparison is given in table 10.

Device	Catadioptric Dimensions (mm)	Reflective Dimensions (mm)
Faraday isolator	500X170	500X170
ITF MMT	800X300	800X450
IMC to Faraday telescope	110X110	110X110
IMC flat mirrors assembly	200X100	200X100
Input power control system (IPC)	300X100	300X100
Area needed for opto-mechanical mounts (mm^2)	93750	93750
Area reserved for the laser beam path (upper part) (mm^2)	115000	115000
Total area (mm^2)	595850	715850
Total area available (Upper part) (mm^2)	708820	708820
Area remaining (mm^2)	112970	-7030

Table 10: Estimation of available space on the upper part of the bench after the integration of all the components needed.

As you can see from this first estimation, it looks that the only telescope that could fit on the SIB is the catadioptric telescope.
NB: in this estimation we have not taken into account the space required to install all the cables that have to reach the bench (for actuators). In order to further investigate the integration of both telescope on the SIB, we started to work on the optical layout of the SIB. For what concern the catadioptric telescope, the last version of the optical layout is presented on figures 19 and 20 and it fits to a bench of 95cm diameter (INJ meeting reference September 5).

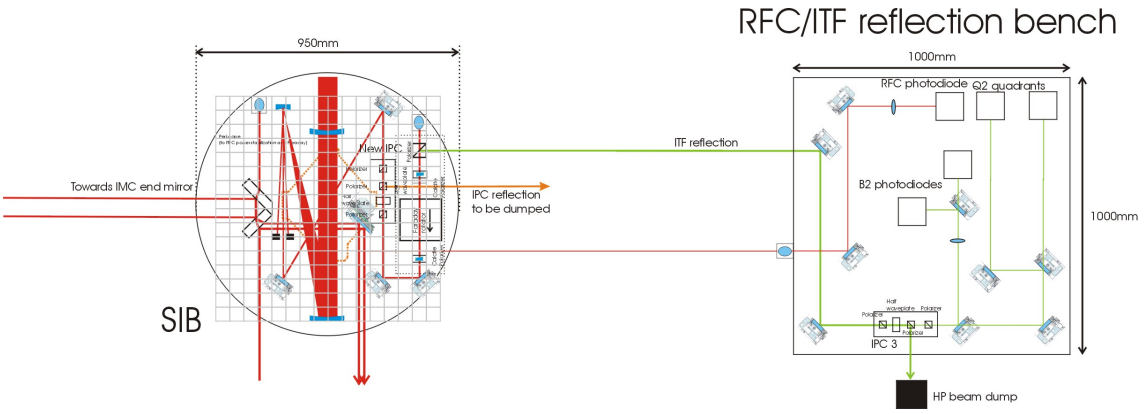

Figure 19: General optical layout of INJ suspended benches (SIB upper part and New ITF/RFC reflection bench)in the case of catadioptric telescope.

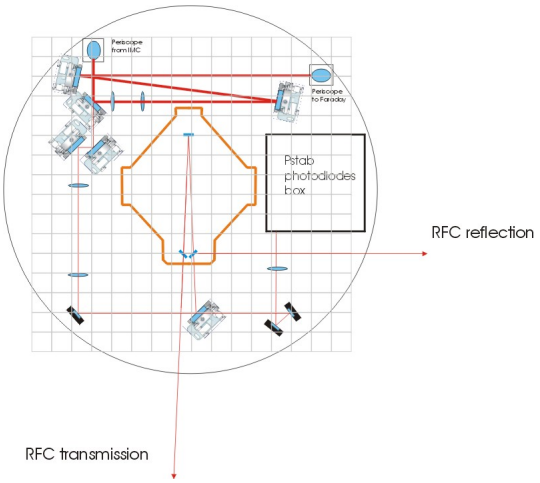

Figure 20: Optical layout of SIB lower part.

For the reflective one, we were not able to properly integrate this telescope on the SIB optical layout as shown on figure 21.

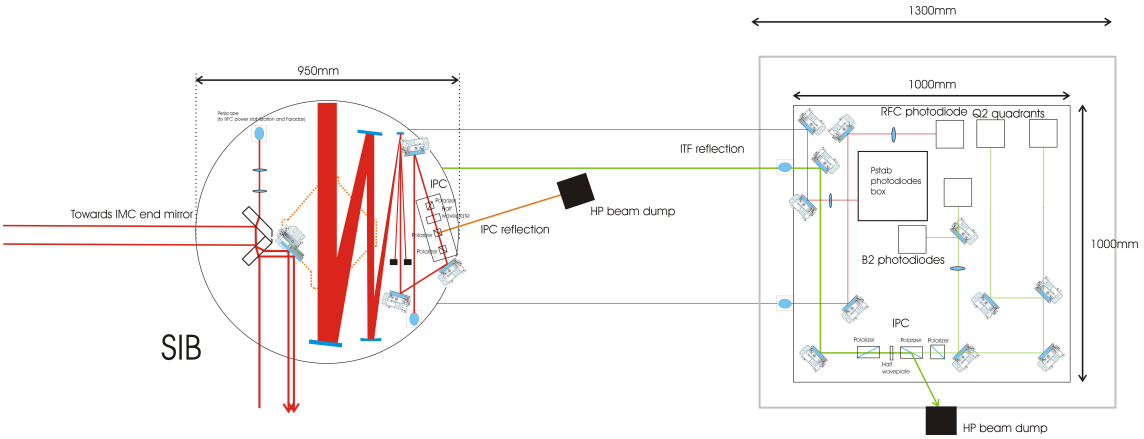

Figure 21: Optical layout of SIB upper part and New ITF/RFC reflection bench) in the case of reflective telescope.

Power stabilization box should be moved in the lower part of the SIB and not be implemented on the new suspended bench as proposed here due to potential problem of beam jitter that could affect the laser power stabilization loop performances [7]. Moreover, having the Faraday isolator (FI) in the lower part of the SIB would make more difficult the work of alignment of the FI alignment more difficult. The only possibility to integrate the reflective telescope on the SIB is to reduce the size of this telescope. In particular the fact that a wedge of 400 urad has been chosen as beam splitter wedge angle enables us to reduce the overall magnification of the telescope. Work has been carried out at APC in order to try to squeeze the reflective telescope and results have been presented at last INJ design meeting (October 13) [8]. On figure 22, you can see the result of reflective telescope size reduction mostly due to the telescope magnification reduction (a factor of 2). The telescope dimension fits the space requirements of the SIB but the matching on the arm cavities falls below 98% which is not acceptable.

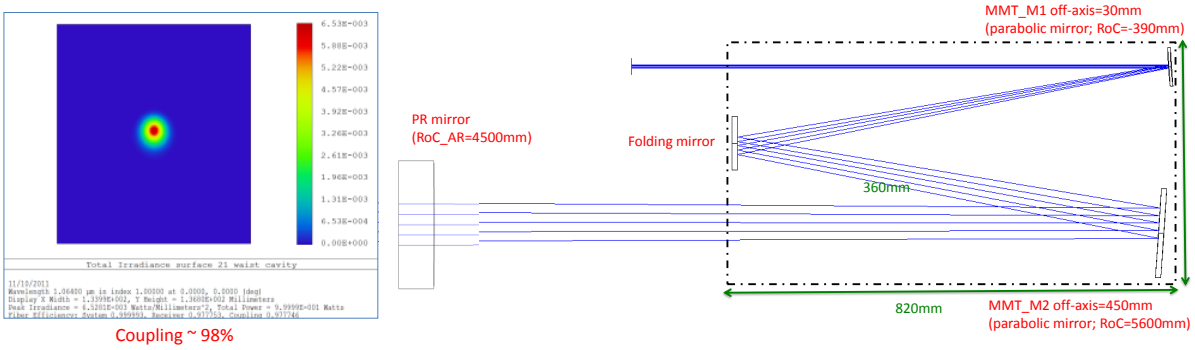

Figure 22: Squeezing the reflective telescope dimension.

5 Diffused and back-reflected light study for INJ

In the 2 configurations proposed, we have to consider the noise coming from the diffused light created by each reflective optic since this noise can spoil the ITF sensitivity either through an up-conversion process or a direct coupling. For the catadioptric telescope, we have also to consider the noise coming from the back-reflection of the 2 faces of the meniscus lens.

5.1 Back-reflected light from the meniscus lens

This question is only related to the catadioptric telescope that uses a lens that is perpendicular to the optical axis thus generating a direct reflection that can be recoupled in the interferometer. A note [9] has been recently released on this topic where linear coupling as well as up-converted noise created by this back-reflection are considered. The projection of these noises on AdV sensitivity curve has been made for both power recycled and dual recycled interferometer. Both Finesse and Optickle codes have been used to compute the effect of back-reflected light noise. More details on the computations are given in VIR-0179D-11[9].

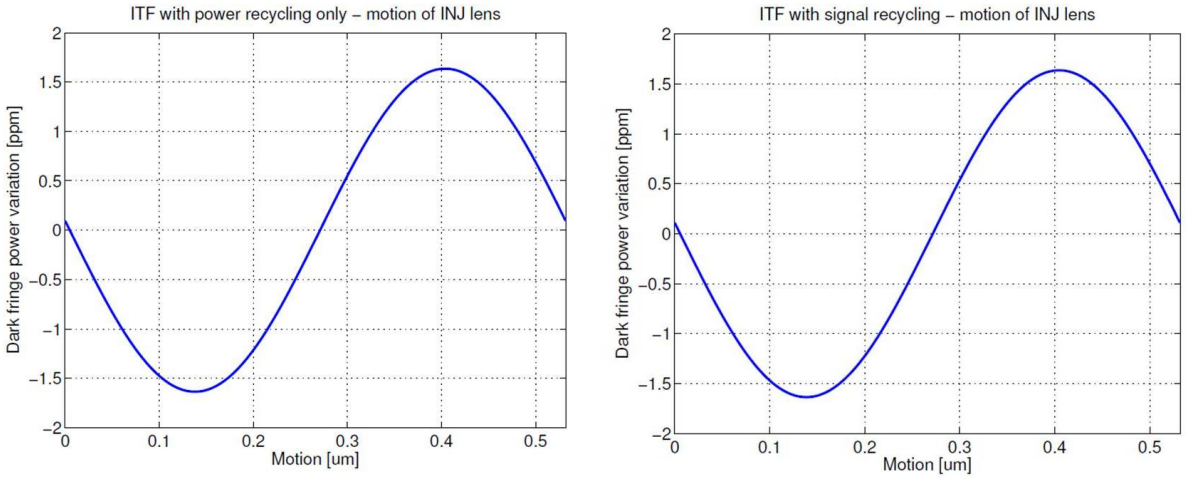

Figure 23: Example of fringes on the dark fringe due to optical element motion over half wavelength (0.532um) for power recycled interferometer (left plot) and dual recycled ITF (right plot).

NB: Each surface (secondary faces of PR and SR and all lens surfaces) have been modeled considering that anti-reflection coating was as high as 50 ppm.

In all configurations each back-reflecting surface is shifted by one entire fringe and the power reaching dark fringe is computed for each position. The typical outcome of these simulations as one can see on figure 23 is that the power at the dark port oscillates with a peak-to-peak amplitude of the order of 1-5ppm of the total dark fringe power depending on the optic that is considered. In the case of dual recycled interferometer the amplitude of the fringes is quite similar to the power recycled interferometer case. The contribution of each face of the meniscus lens has been considered and it has been found that one face is mainly contributing (the face with the smaller RoC).

5.1.1 Up-converted noise

Projections of this noise on AdV sensitivity curve is given for the power recycled interferometer is given in figure 24.

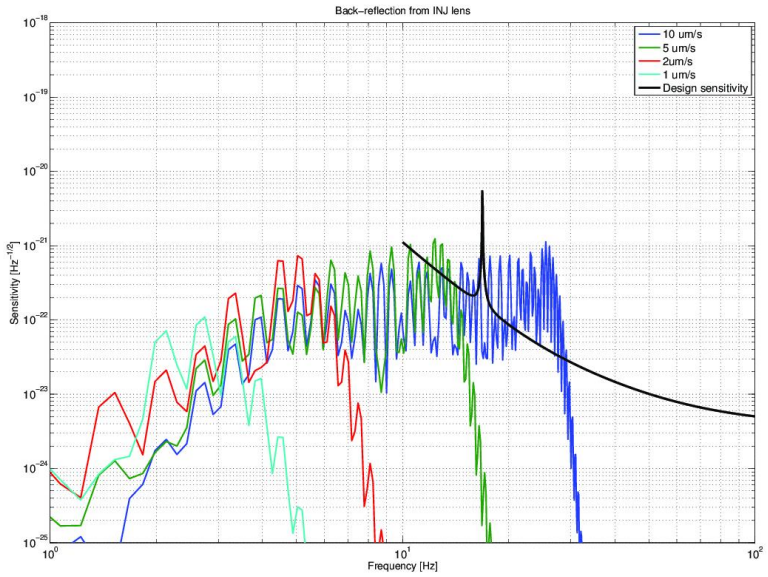

Figure 24: Power recycled interferometer. Projection of up-converted back-reflected light in the case of injection MMT lens moving. The motion is peaked at 300 mHz and the total RMS is the one quoted in the legend.

Results for the dual recycled interferometer are given in figure 24.

In both cases (PR ITF and Dual recycled ITF), if the RMS motion around 300 mHz is lower than 2 μm/s the noise does not enter inside the detection bandwidth. The residual motion in normal condition is much lower than this requirement, since in [10] it is measured that the RMS speed of the payload is lower than 0.1 μm/s for a full super-attenuator chain. Therefore the requirement is fulfilled in normal conditions. G factor for each optic has been computed using the definition given in [11] and are given in table 11 considering an anti-reflective coating reflectivity of 100 ppm.

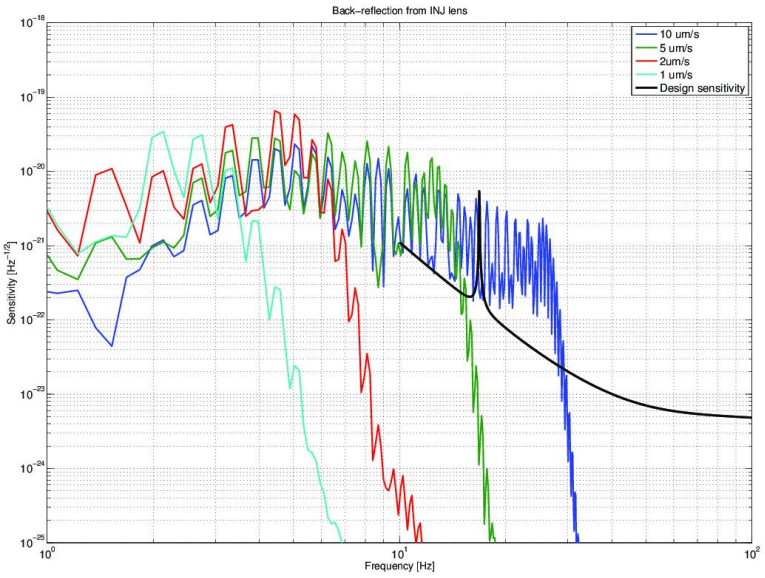

Figure 25: Dual recycled interferometer. Projection of up-converted back-reflected light in the case of injection MMT lens moving. The motion is peaked at 300 mHz and the total RMS is the one quoted in the legend.

Configuration	Surface	G factor (AR=100ppm)
Power recycled ITF	Meniscus lens INJ (face 1)	$4.2.10^{-21}$
	Meniscus lens INJ (face 2)	$1.4.10^{-21}$
Dual recycled ITF	Meniscus lens INJ (face 1)	$9.9.10^{-21}$
	Meniscus lens INJ (face 2)	$2.8.10^{-21}$

Table 11: G factors of each face of meniscus lenses in the case of Power Recycled and Dual recycled interferometers considering a reflectivity of the anti-reflective coating of 100ppm. Face 1 is the one with radius of curvature of 2900 mm, face 2 the one with radius of curvature of 1038 mm.

5.1.2 Linear coupling

The effect of direct modulation of the back-reflected light by a motion of the bench at a frequency which is inside the detection bandwidth has been simulated with Finesse. The worst coupling is obtained when the microscopic distance between the interferometer and the back-reflecting object is tuned at half fringe. In this condition the slope of the induced fringes is maximum and the worst coupling is obtained. The transfer function between a lens motion and dark fringe power is computed and calibrated in terms of detector sensitivity. The design sensitivities for power-recycled only (125 W input power) and dual-recycled (125 W input power) can then be used to compute the requirements for the bench and lens motions. Results for both configurations of the ITF are given in figure 26.
NB: No safety factor is considered in these plots.

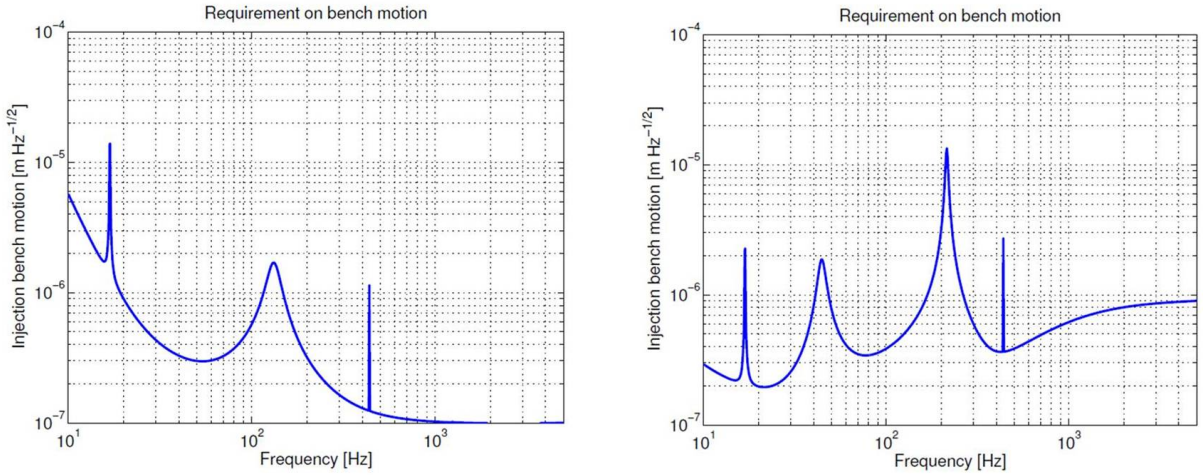

Figure 26: Requirements for SIB for Power recycled interferometer (left plot) (no safety margin is applied).; Requirements for SIB for Dual recycled interferometer (right plot) (no safety margin is applied).

As shown in the two plot, the requirements are quite relaxed for the SIB because assuming a safety factor of 10 the bench must move less than 10^{-8}m/$sqrt(Hz)$ at all frequencies and the Virgo bench has shown to move much less than that (see figure 37-right).
NB: These numbers are computed in the case of 50 ppm of back-reflection of the AR coating and scale proportionally to the square root of the power that is recoupled inside the interferometer. This means that if we want to consider a back-reflection of the optics of 100ppm the requirements should be divided by square root of 2.

5.2 Back-scattered light from telescopes' optics

First of all what is important in this study is to compute the fraction of diffused light by an optical element that is recoupled in the ITF. Hereafter we will call this quantity fsc. In order to compute this factor, we used 2 methods:
- An analytical model already used to compute the contribution of each optic of Virgo's end benches to the diffused light noise [12].
- The second based on FFT code [13].
Moreover Zemax software has been used to make simple cross-checks of the analytical model and make a simple computation since we found a non-convergence of the results obtained when a huge number of interfaces is considered (see next paragraphs).

5.2.1 Estimating the recoupling of diffused light using the analytical model

Principle

In this paragraph, we introduce the principle of the analytical calculation of diffused light recoupling. Complete details of the method can be found in the Virgo note VIR-0375A-10 [12]. The model enables to compute the quantity of the diffused light from an optic placed on an external bench that recombines to the main mode of the AdV cavities (this quantity is called f_{sc}). It is based on a treatment of diffused light based on geometrical optics. A photon is emitted from a diffusing surface and propagated through the external benches and the cavities and is considered recoupled if it does not superate the various optical apertures through the propagation. In the following, we give further details about the method.

A single photon emitted from the diffusing surface can be described by its emitting position: $\begin{pmatrix} x \\ y \\ 0 \end{pmatrix}$ (the origin along z optical axis is taken at the emitting source) and its normalized direction $\begin{pmatrix} u \\ v \\ w \end{pmatrix}$. In reality, the recoupling problem gets a cylindrical symmetry and we can limit the calculation to small polar angles (paraxial like approximation). The relevant parameters will then be the distance from optical axis r and the normalized direction vector $\begin{pmatrix} \phi cos(\theta) \\ \phi sin(\theta) \\ 1 \end{pmatrix}$ (see figure 27).

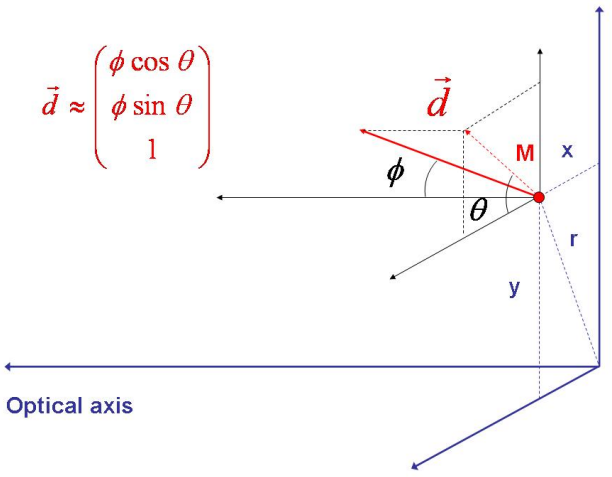

Figure 27: Description of the different parameters characterizing the diffusing photons.

For a photon described by those parameters, we define the boolean recoupling function $F(r, \theta, \phi)$ which is equal to 1 if the photon is recoupled, 0 otherwise. The relative power recoupled by a diffusing surface covering the whole beam of intensity I(r) can be written:

$$f_{sc} = \int_0^{\infty} \int_0^{2\pi} rI(r)d^2P(r)d\alpha dr$$

Where:

$$d^2P(r) = \int_0^{2\pi} \int_0^{\pi/2} \frac{dP}{d\Omega} sin(\phi)F(r, \theta, \phi)d\theta d\varphi$$

It comes:

$$f_{sc} = 2\pi \int_0^{\infty} \int_0^{2\pi} \int_0^{\pi/2} rI(r) \frac{dP}{d\Omega}(r,\phi) Sin(\phi) F(r,\theta,\phi) dr d\theta d\phi$$

In the above formula, $\frac{dP}{d\Omega}(r,\phi)$is the quantity of diffused light emitted by the considered surface per unit of steradian. It is linked to the BRDF of the surface by the formula:

$$BRDF(r,\phi) = \frac{1}{P_i cos(\phi)} \frac{dP}{d\Omega}(r,\phi)$$

.

About diffusion models:

In the following we will take usually a constant BRDF model that corresponds to the hypothesis that the diffusing surfaces are Lambertian. In other means: $\frac{dP}{d\Omega}(r,\phi) = \frac{\alpha}{\pi} cos(\phi)$where α is the Total Integrated Scattering (TIS) of the surface.

The hypothesis of Lambertian diffusion is valid in the case we have to consider only **large angle diffusion** (diffusing photons emitted by angles larger than a few degrees with respect to the specular reflection). This condition is perfectly respected in the case of the different mirrors of the two different MMTs. More generally, this condition is respected for **common optics** of the external benches as much care is taken to tilt them by few degrees to correctly dump their specular reflection. In the case of optics close to normal incidence (such as the meniscus lens) this model is no more accurate and the results will, of course, depend on the angular dependence of the BRDF considered. In the following, to study the meniscus case, we will take BRFD extracted from realistic PSDs as input of the calculation.

About calculation of the recoupling function$F(r,\theta,\phi)$:

As said before, we realize the propagation of the photon inside the optical system placed on the external bench. Then the photon is propagated trough the Virgo cavities. The photon is considered resonant if it couples through both systems. It means that it should not superate the different optical apertures. In the case of the cavity propagation, the photons should make a certain number of round trips (this will be discussed further) without getting out of the mirror coatings. Therefore, for a given photon emitted by the scattering surface, we calculate its coordinates x_i, y_i, z_i in the plane of the optical component number i and check if ($x_i{}^2$+ $y_i{}^2$)< a_i were a_i is the radius of this component. The coordinates x_i, y_i, $z_i$propagating the photon through the optical system by geometrical optics (further details of the method can be found in [12]).

Cross-check with Zemax

In this section we present a cross check of the results of the analytical code with Zemax software. As Zemax may not be used in a simple way to consider cavity recoupling (due to the precision of the calculation needed, see [15] and [14] for more details) we consider a simplified case presented in figure 28. In this case, we calculate the quantity of light emitted by a diffusing element (TIS=1) placed after the recycling mirror that can reach by back-scattering the end mirror. This situation would correspond to the recoupling to the cavity considering only a half round-trip.

Figure 29 gives the f_{sc} calculated as a function of the position of the diffusing element from the PR mirror. We observe the same consistent results from two methods with a maximum recoupling of $3.5.10^{-4}$ located around the waist position.

Convergence of the analytic code.

As mentioned previously, simulations made with Zemax suffer from a problem of convergence and the quantity of recoupled light drops systematically as a function of the considered round-trips. We checked the convergence of the analytical code by calculating f_{sc} for the situation presented in figure 28 as a function of the considered round trips. Results of the analytical code are presented in figure 30. We observe that the simulation results does not change anymore when more that 4 round-trips are considered as light is simply recoupled to the cavity mode. Anyway, in the following, all calculations will be made considering 15 round-trips.

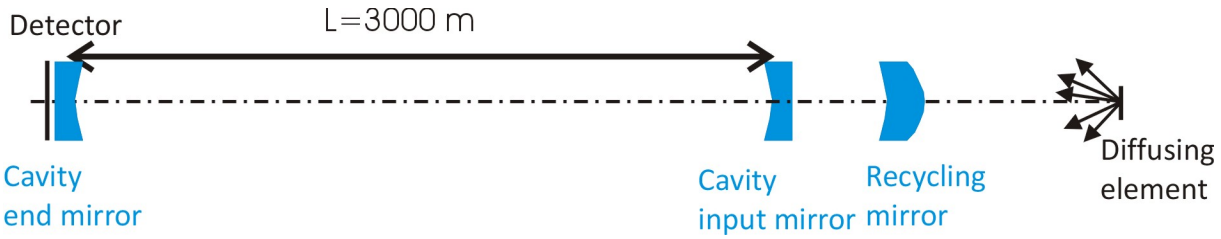

Figure 28: Setup considered for the comparison of the two calculation methods. The light emitted from a diffusing element located after the PR mirror is considered recombined if it reaches the end mirror.

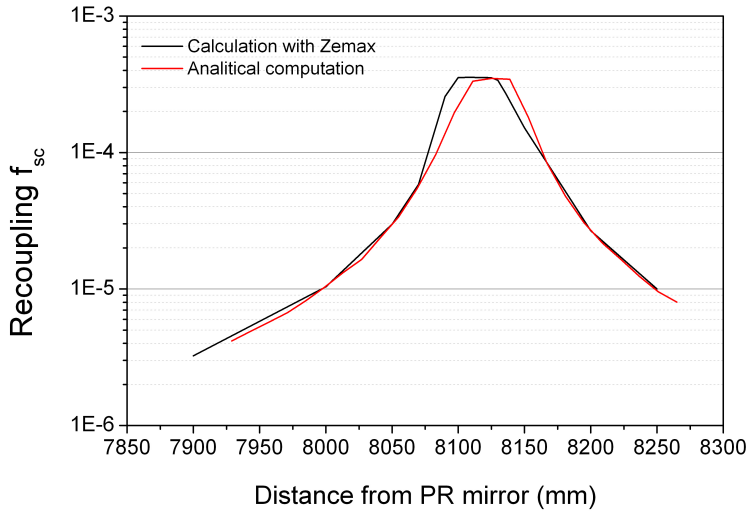

Figure 29: Recoupling as a function of the distance between the diffusing element and the PR mirror.

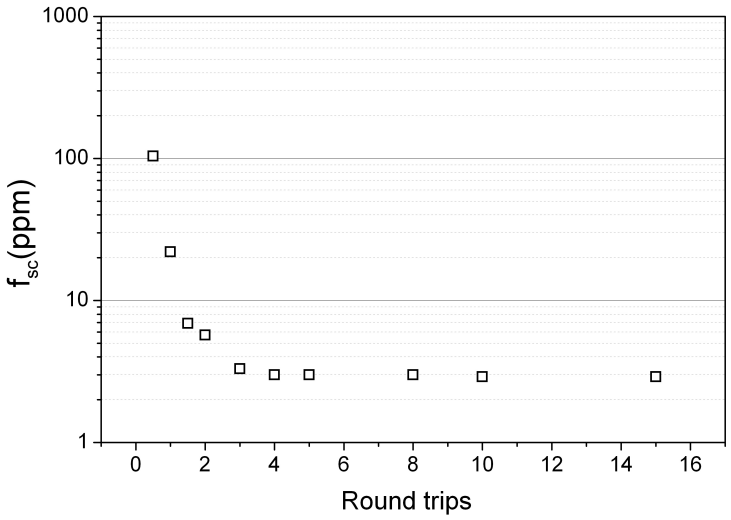

Figure 30: Recoupling f_{sc} calculated with analytical code as a function of round-trip inside cavities.

5.2.2 Estimating the recoupling of diffused light using the FFT code: principle

A study has been made using FFT propagation code in order to cross-check with the ray tracing and analytical approaches. The diffused light source is generated in simulation by passing a TEM00 beam (which the HG base of the arm cavity mode) through an optical diffuser. This diffuser is a phase mask which is a randomly generated phase map with a flat PSD (lambertian diffuser) having an rms of greater than 4 radians to have a completely diffusing object. An amplitude image of the beam in the near field and far field is shown in figure 31.

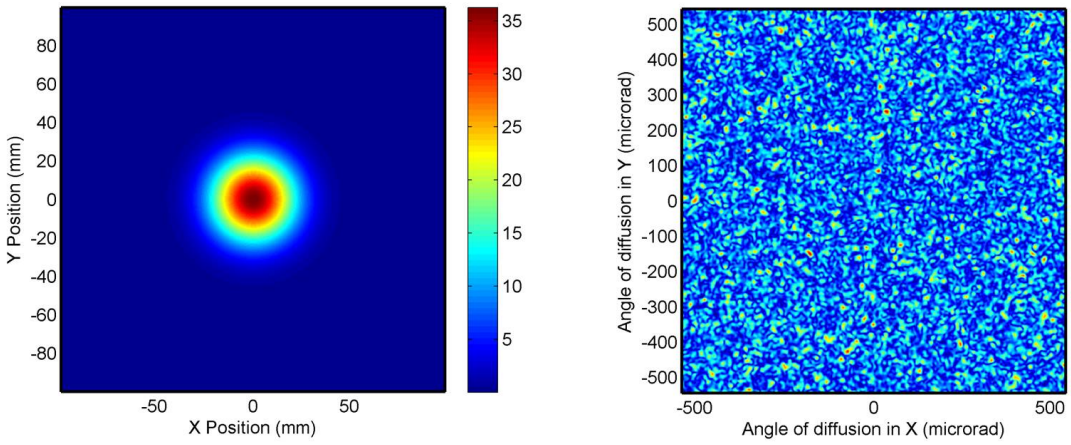

Figure 31: (left) Amplitude image of Gaussian beam just after passing through phase grating. (right) Amplitude image in the focal plane of 1m lens. This image gives directly angle of diffusion of light (axes in units of microradians).

In order to increase simulation speed it is supposed that the coupling of diffused light in a locked cavity is equivalent to the overlap integral between the diffused light source and the cavity mode. Figure 32 shows the validation of this assumption.

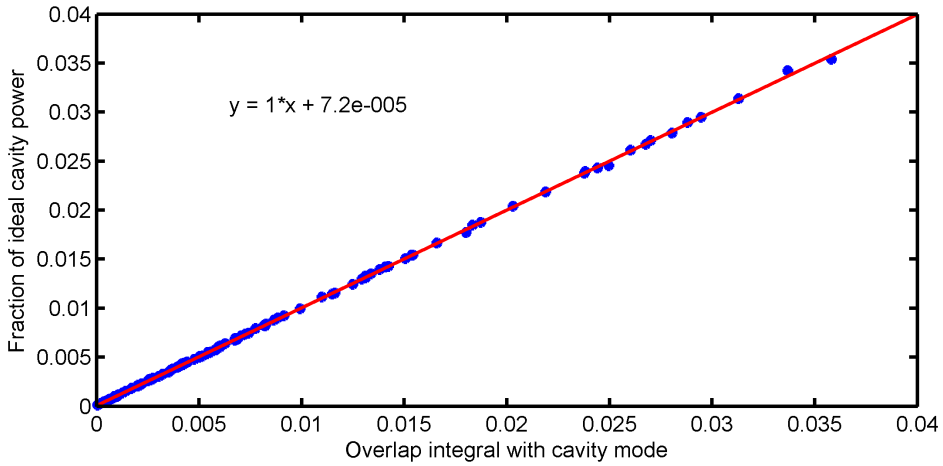

Figure 32: Comparison between diffused light power in locked cavity and overlap integral of diffused light source and cavity mode. Each blue point corresponds to different random diffuser.

We may therefore use an overlap integral to calculate the coupling of a lambertian diffuser into the AdV Virgo arm cavities. The result for 1000 random diffusers is shown in figure 33. We see that there is a broad distribution in coupling. However the coupling does not exceed 5.10^{-10}. This is compatible with the value of 8.10^{-10} in table 12 obtained with the analytical solution.

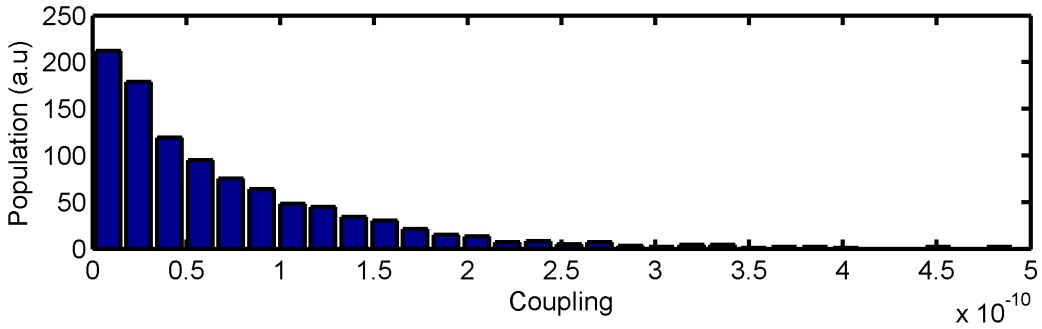

Figure 33: Histogram of coupling of lambertian diffused light source into cavity mode for 1000 different random diffusers.

5.2.3 Fraction of diffused light recoupled in the interferometer

Catadioptric telescope

First we estimated the contribution of each optical element of the telescope using Lambertian distribution (perfectly diffusing surface) as diffusion law. The results are given in table 12.

Optical element	f_{sc} (TIS=1)	f_{sc} (with TIS=10ppm for ML and 500ppm for parabolic mirrors)
Meniscus lens INJ (face 1) (RoC=1038mm)	8.10^{-10}	8.10^{-15}
Meniscus lens INJ (face 2) (RoC=2900mm)	$8.20.10^{-10}$	$8.20.10^{-15}$
Parabolic mirror M1	$8.60.10^{-10}$	$4.3.10^{-13}$
Parabolic mirror M2	$1.87.10^{-7}$	$9.35.10^{-11}$

Table 12: Fraction of scattered light recoupled in the ITF for the catadioptric telescope in case of a Lambertian distribution of diffused light.

As one can see, the computation has been done considering a Total Integrated Scattering (TIS) value equal to 1. Then in order to obtain the final f_{sc} of each optic we multiplied this number by a typical TIS of 10ppm for super-polished spherical surfaces (meniscus lens faces) and by a TIS of 500ppm for parabolic mirrors (typical value measured on Virgo parabolic mirrors). We also estimated f_{sc} for a different diffusion law especially for the meniscus lens. The Power Spectral Density (PSD) and its corresponding bidirectional reflectance distribution function (BRDF) is shown on figure 34. The result of this simulation is given in table 13.

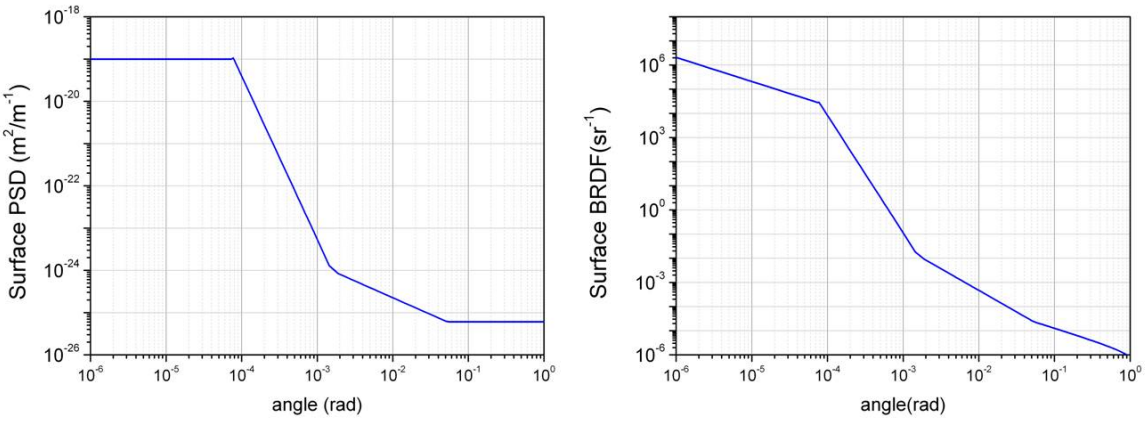

Figure 34: Left plot: Typical Power Spectrum Density (PSD) of a super-polished optic (corresponding to about 2nm rms). Right plot: corresponding BRDF.

We have also performed a third simulation that is considered to be very conservative, we computed with Zemax the quantity of light diffused by each optical element of the catadioptric telescope that reaches the end mirror. The principle of this simulation is described on figure 35.

Each surface of the optics of the telescope is taken one after the other and is considered to be a totally diffusing surface (TIS=1). This element is diffusing back light towards the Interferometer. Then we measure the quantity of light that reaches the end mirror where a detector is located.

Optical element	f_{sc}
Meniscus lens INJ (face 1) (RoC=1038mm)	$4.2.10^{-10}$
Meniscus lens INJ (face 2) (RoC=2900mm)	$3.7.10^{-9}$

Table 13: Fraction of scattered light recoupled in the ITF for the meniscus lens faces in case of a typical diffusion of a super-polished surface.

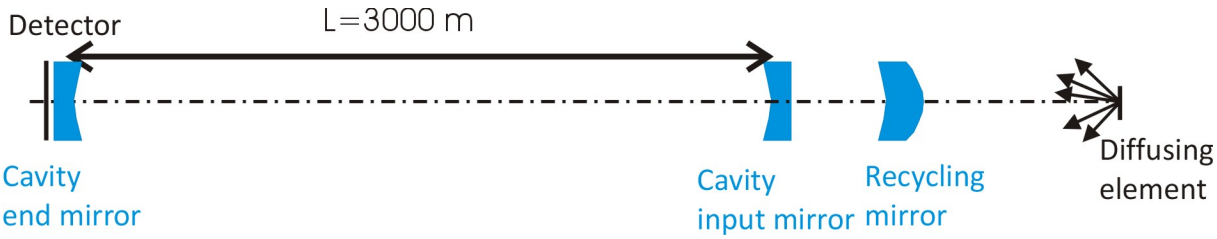

Figure 35: A diffusing surface from the telescope is diffusing the light back towards the long cavity end mirror where we have placed a detector. The power we find is an upper limit of f_{sc}.

Optical element	f_{sc} (TIS=1)	f_{sc} (with TIS=10ppm for ML and 500ppm for parabolic mirrors)
Meniscus lens INJ (face 1) (RoC=1038mm)	$1.9.10^{-8}$	$1.9.10^{-13}$
Meniscus lens INJ (face 2) (RoC=2900mm)	$6.5.10^{-9}$	$6.5.10^{-14}$
Parabolic mirror M1	2.10^{-9}	1.10^{-12}
Parabolic mirror M2	9.10^{-6}	$4.5.10^{-9}$
Optical element placed at the waist	$3.5.10^{-4}$	$1.75.10^{-7}$

Table 14: Fraction of scattered light reaching the 3km-arm end mirror for each optical surface of the catadioptric telescope in the case of a Lambertian diffusion law.

In table 14, we present the results obtained. As once can see, we also considered in the upper limit a diffusing element placed at the waist of PR curved mirror (worst case scenario). In this case we could find that the fraction of scattered light recoupled in the ITF is of the order of 1.75 10^{-7}. Note that this number is at least 2 orders of magnitude above the value computed for the meniscus lens in the case of a peaked BRDF law (see table 13), so taking this number in consideration to compute the projection of diffused light noise from ITF mode matching telescope is considered to be very conservative and this is what we will use in section 5.2.4 to compute the projection of diffused light noise on AdV sensitivity curve.

Reflective telescope For what concern the reflective telescope, results of the computation are given in table 4. As one can see, there is not much difference between this configuration and the catadioptric telescope. As in the previous case the most critical element is the parabolic mirror where the beam size is smaller.

Optical element	f_{sc} (TIS=1)	f_{sc} (with TIS=500ppm for parabolic mirrors)
Parabolic mirror M1	$3.9.10^{-9}$	1.95^{-12}
Parabolic mirror M2	$2.5.10^{-7}$	$1.25.10^{-10}$

Table 15: Fraction of scattered light recoupled in the ITF for each parabolic mirror of the reflective telescope in the case of a Lambertian diffusion law.

Numbers given in table 15 are very similar to the ones given in table 12. In conclusion, both solutions are satisfying from the diffused light point of view. Nevertheless, the meniscus lens contribution is the limiting element considering a realistic diffusion law (see figure 34) but we are still about 2 orders of magnitude below the worst case scenario a diffusing element placed at PR mirror waist.

5.2.4 Projection of diffused light noise coming from ITF MMT optics

The optical phase noise $\delta\varphi(t)$ induced at the ITF input port by a diffusing object moving of $\delta x(t)$ is written as follow:

$$\delta\varphi\left(t\right) = \sqrt{f_{sc}}\sqrt{\frac{P_r}{P_{in}}} sin\left(\frac{4\pi}{\lambda}\delta x(t)\right)$$

P_r is the power reflected by the ITF, P_{in}, the power at the ITF input port.

The phase noise in the frequency domain is:

$$\delta\varphi\left(f\right) = TF(\delta\varphi\left(t\right))$$

As explained in [16], the phase noise is related to frequency noise by the following formula:

$$\delta\nu_{in} = f\delta\varphi$$

The second stage of frequency stabilization will reduce the frequency noise at the ITF input port by G_{SSFS}, so:

$$\delta\nu = \delta\nu_{in}/G_{SSFS}$$

The frequency noise induced at the ITF input port is equivalent to a differential arm length that can be written:

$$\tilde{h} = \frac{\delta\nu}{\nu_{las}} CMRF$$

Where $CMRF$ is the common mode rejection factor and ν_{las}, the laser frequency.

$$\tilde{h} = \frac{f\delta\varphi}{\nu_{las} G_{SSFS}} CMRF$$

If δx is small ($<\lambda/30$) this formula can be approximated by:

$$h\,(f) = G\frac{4\pi}{\lambda}\delta x(f)$$

where

$$G = \frac{f}{\nu_{las} G_{SSFS}} CMRF \sqrt{f_{sc}} \sqrt{\frac{P_r}{P_{in}}}$$

In order to make this computation, we asked to ISC to provide the *CMRF* of AdV and the SSFS gain. The gain of the SSFS, is expected to follow the law: G_{SSFS}=400 * (500/f)^2. The CMRF is shown on figure 36. To make the projection, we considered the worst case: Losses assymetry=-50ppm and finesse asymmetry=-2%).

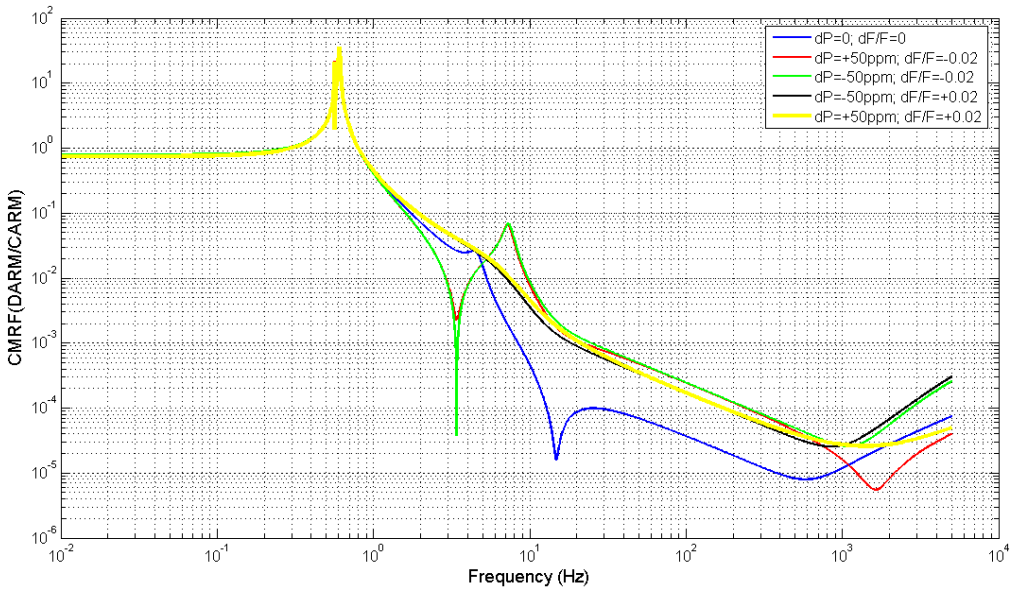

Figure 36: Common mode rejection factor (CMRF) for AdV.

The residual horizontal displacement of Virgo SIB, presented on figure 37, has been reconstructed using reference cavity error signal in Fall 2011 during a campaign of measurements.

To make the projection we also considered that the power incident on the ITF Pin is 125 W and the power reflected by the ITF Pr is 0.2* Pin. The projection of diffused light noise for INJ telescope on AdV sensitivity curve is given on figure 38. To make this projection we considered the worst case scenario: a diffusing element placed at the beam waist after PR mirror with a total integrated scattering of 500ppm as computed in table 14 in the case of high micro-seismic activity. As shown on the plot, we are order of magnitude below AdV sensitivity. This means that for INJ telescope both configurations could be chosen. Note that in the projection, we also considered double and triple bounce contributions.

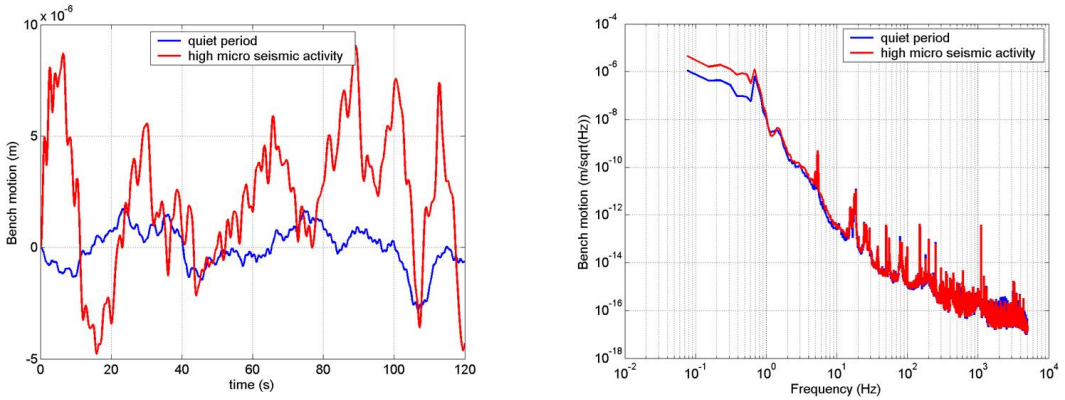

Figure 37: VIRGO SIB horizontal motion (estimated using IMC length noise measured with RFC error signal) in case of high (red) and low micro-seismic (blue) activity.

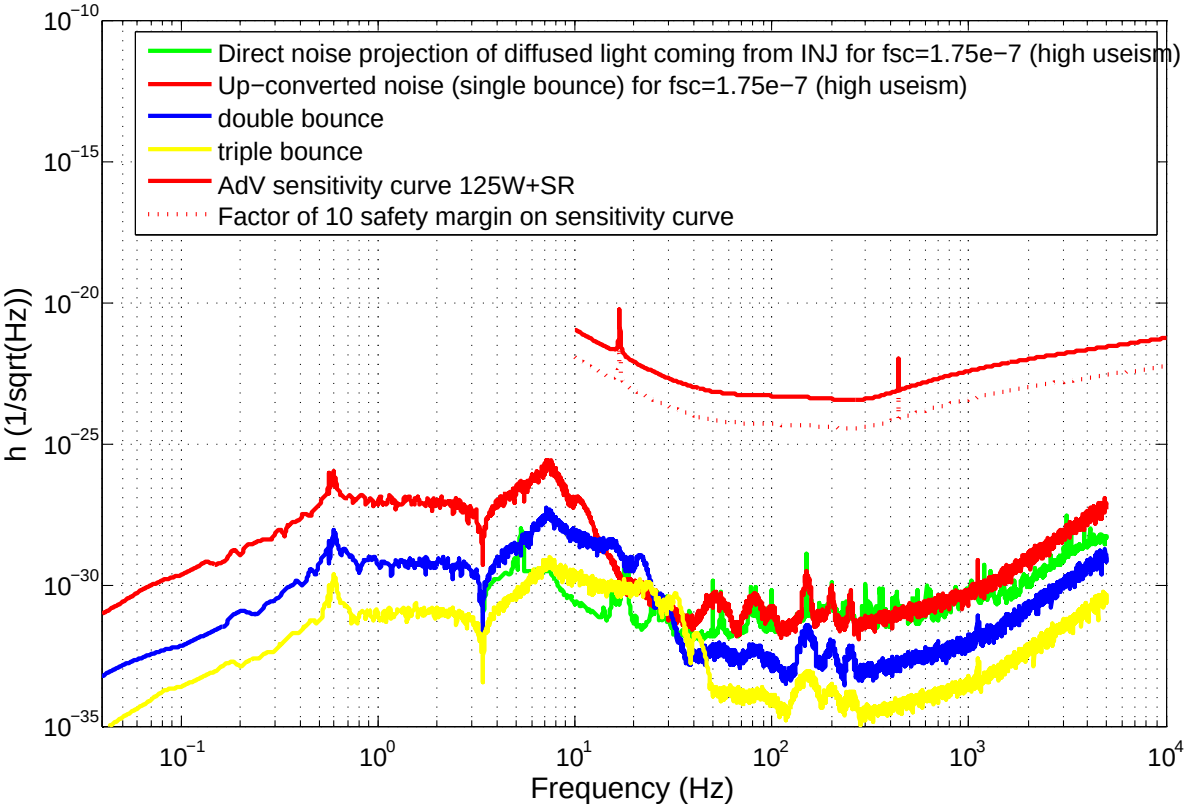

Figure 38: Projection of diffused light noise coming from INJ telescope in the case of high micro-seismic activity.

5.3 Dumping back-reflected and back-scattered light not recoupled in the ITF

It looks reasonable to ask where is going the light that is reflected or scattered and that is not recoupled in the interferometer because this light could also spoil the interferometer sensitivity and how we dump it. Some studies have been done using Zemax and we could conclude that it is very important to properly place the baffles in the central Interferometer and between the ITF and INJ tower to dump efficiently all this light. With a proper baffling design, we can dump this spurious light and avoid possible troubles. An example of baffling between PR mirror and INJ tower is given on figure 39. This work will be done by the group responsible for the baffles design in AdV.

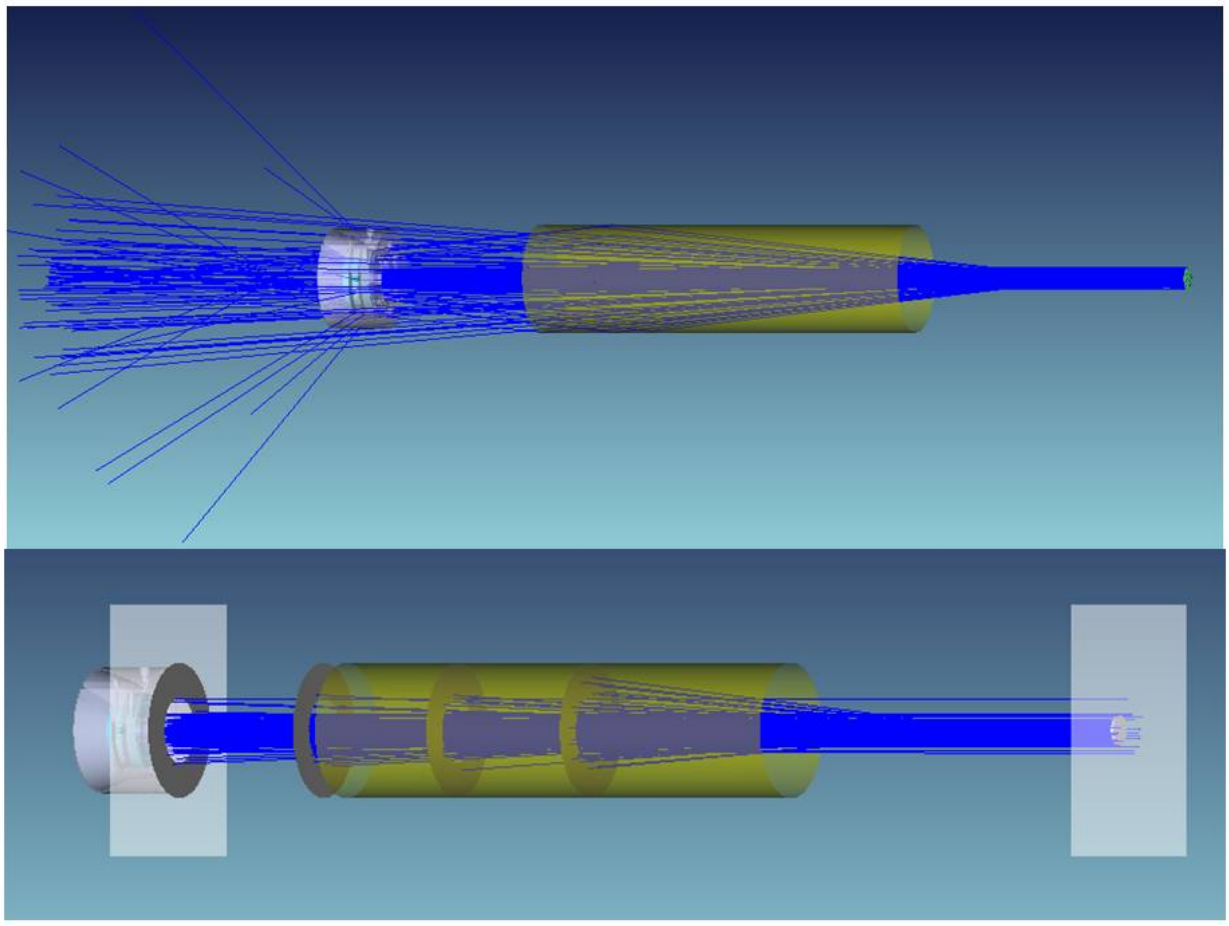

Figure 39: Projection of diffused light noise coming from INJ telescope in the case of high micro-seismic activity.

In any case, we can make a simple computation based on the definition of Figure of Merit 1 (FOM1)(see OSD chapter). We should have at maximum 100ppm (AR coating reflectivity) for each face of the meniscus lens that can fall out of the ITF optics clear aperture. If we consider P_{in}=1W incident power on those faces, we have : P_{in}*100ppm=0.1mW. This number has to be compared with FOM1 for the central ITF that is equal to: P_{out}=1.4ppm*17*G_{rec}*P_{in}=1.4ppm*17*40*P_{in}=0.95mW where 17 is the number of surfaces in the central ITF, 1.4ppm is the amount of light diffused by the mirrors at large angle (due to micro-roughness), G_{rec}, is the recycling gain. In conclusion the amount of scattered light coming from the meniscus lens that has to be dumped is 9.5 times lower than the amount of scattered light that has to be dumped in the central ITF so this should not be a problem and can be dumped by using appropriate baffles.

6 Conclusion

All the studies we made so far were focused on a trade-off analysis between the two MMT configurations. The first configuration is based on a two mirrors off-axis parabolic telescope and a meniscus lens. The design of the second configuration, essentially made by reflective optics, has been motivated by the use of a lens in the catadioptric telescope that could affect AdV performances due to the fact that this optic is perpendicular to the laser beam axis. Several studies have been carried out: performances of the telescopes, tolerancing, space constraints and back-reflected/back-scattered light problems. Concerning the back-scattered light, we are far to limit the AdV sensitivity as when taking an important safety margin (high total integrated scattering, typical Virgo suspended benches motion in case of high micro seismic activity, conservative condition (reaching the end mirror)) we are still more than three orders of magnitude below the reference AdV sensitivity curve. Concerning the back-reflected light of the meniscus lens for the catadioptric telescope, the conclusion is similar to the previous one. The tolerancing analysis showed that the requirements on the optics displacements or the SIB displacements are quite similar between for both configurations, and are realistic. However, the limited space available on the suspended bench implies that the catadioptric telescope, that is more compact than the reflective one, is the only configuration that fits the space requirements. Taking into account all these elements, the catadioptric telescope is the most suitable configuration for the INJ MMT. Further work is still needed, in collaboration with the OSD group, in order to refine the work on pick-off beams extraction. Magnification of the telescope has been reviewed to relax the optical/mechanical constraints of the telescope and allow us to have a bigger beam in the Faraday isolator to be able to fulfill the requirements given in INJ Final design report.

References

[1] E. Genin, *AdV: MSRC configuration: preliminary study of input MMT*, VIR-0114A-11, (2011). 2

[2] R. Day, E. Genin, V. Fafone, G. Vajente, J. Marque, *AdV design: MSRC case (summary)*, VIR-0139A-11, (2011).

[3] E. Genin, *AdV MSRC: progress on pick-off extraction*, VIR-0166A-11, (2011). 2

[4] C. Buy, M. Barsuglia, *AdV input/output mode matching telescopes for the MSRC. Update of the preliminary study*, DET/INJ joint meeting on telescopes, (2011). 3

[5] E. Genin, *AdV: MSRC configuration: preliminary study of input MMT*, VIR-0114C-11, (2011). 4

[6] P. La Penna, O. Francois, J. Marque, E. Genin, *Note on Virgo parabolic telescope: design, installation and commissioning*, VIR-0504A-10, (2010). 15

[7] Personal communication with Frederic Cleva. 18

[8] C. Buy, M. Barsuglia, *AdV INJ MMT optical studies*, INJ design meeting, October 13, 2011, https://workarea.ego-gw.it/ego2/virgo/advanced-virgo/inj/restricted/meetings/adv-inj-13-10-2011/Meeting_13_10_11_BUY_v2.pdf 20

[9] G. Vajente, *Simulation of back-reflection from injection and detection mode-matching telescopes*, VIR-0179D-11, (2011). 20

[10] S. Braccini, *Measurement of suspension performance*, VIR-NOT-PIS-1390-191 (2002), https://tds.ego-gw.it/ql/?c=1339 21

[11] B. Canuel, I. Fiori, J. Marque, E. Tournefier, *Diffused light mitigation in Virgo and constraints for Virgo+ and AdV*, VIR-0792A-09, https://tds.ego-gw.it/ql/?c=7118 22

[12] B. Canuel, E. Genin, J. Marque, P. Ruggi, *Towards the choice of Mode matching telescopes configuration*, VIR-0546A-11, https://tds.ego-gw.it/ql/?c=8602 22

[13] R. Day, *Update on Diffused light from MMT optics with FFT code*, VIR-0549A-11, https://tds.ego-gw.it/ql/?c=8605 24, 25, 26

[14] E.Genin ,*AdV MSRC: Study of back-scattered light from MMT telescope optics: catadioptric telescope*, https://workarea.ego-gw.it/ego2/virgo/advanced-virgo/inj/restricted/meetings/det_inj_telescopes_17062011/DETINJMMT_Genin_17062011.pptx/ 24

[15] B.Canuel, E.Genin, *Study of back-scattered light from MMT telescope optics- first comparison Zemax-analytical code*, https://workarea.ego-gw.it/ego2/virgo/advanced-virgo/inj/restricted/meetings/det_inj-meeting_04072011/DETINJMMT_Canuel_04072011.pptx/ 26

[16] E. Tournefier, *Back-scattering by the optical benches: results from Virgo and constraints for AdV*, VIR-0070A-08, https://tds.ego-gw.it/ql/?c=2083 26

32